Digital Signal Processing 58 (2016) 102–114

Contents lists available at ScienceDirect

Digital Signal Processing

www.elsevier.com/locate/dsp

Real-valued DOA estimation for a mixture of uncorrelated and coherent sources via unitary transformation

Weijian Si, Pinjiao Zhao, Zhiyu Qu *, Yan Wang

Department of Information and Communication Engineering, Harbin Engineering University, Harbin 150001, PR China

ARTICLE INFO

Article history:
Available online 3 August 2016

Keywords:
Real-valued DOA estimation
Uncorrelated source
Coherent source
Uniform linear array (ULA)
Augmented matrix

ABSTRACT

This paper presents a novel real-valued DOA estimation method to handle the scenarios where both the uncorrelated and coherent sources coexist. More specifically, an augmented matrix is constructed and then transformed into a real-valued version for the DOA estimation of uncorrelated sources by utilizing the unitary transformation, which allows an extension of the effective array aperture. Afterwards, an oblique projection operator is employed so that the contributions of the uncorrelated sources are removed. Finally, a real-valued coherent augmented matrix is constructed to estimate the remaining coherent sources. In addition, the fading coefficients are estimated by adding penalties to a constraint quadratic minimization problem, which guarantees the stability of the solution. Compared with the existing partial real-valued and complex-valued DOA estimation methods for a mixture of uncorrelated and coherent sources, the proposed method offers favorable performance in terms of both estimation accuracy and computational efficiency. Furthermore, our method makes it possible to resolve more sources than the number of sensors. Simulation results demonstrate the effectiveness and notable performance of the proposed method.

1. Introduction

Direction of arrival (DOA) estimation has been a research issue of great interest in many application fields, including radar, communication systems and seismology [1,2]. Compared with the maximum likelihood (ML) method [3], the multiple signal classification (MUSIC) method [4] is known as a classical subspace-based method for DOA estimation as well as the estimation of signal parameter via rotation invariance techniques (ESPRIT) [5], which can provide satisfactory performance for uncorrelated sources without large computational load. However, in practical environments, sources from the identical target may go through reflection from various surfaces, and hence the received sources may be a mixture of uncorrelated and coherent sources. In such environments, the methods mentioned above would suffer from performance deterioration owing to the rank deficiency of the array covariance matrix caused by the multipath propagation [6].

In order to solve the aforementioned problem, several decorrelation methods have been presented. Spatial smoothing (SS) technique [7,8] is a remarkable decorrelation method, wherein the whole array is segmented into a series of subarrays and the subarray covariance matrices are averaged to combat the rank deficiency. Pillai et al. proposed an improved SS technique referred to as the forward/backward spatial smoothing (FBSS) technique [9], and the minimum number of sensors required by FBSS is reduced to $[3K/2]$ as compared with $2K$ for the SS method (K represents the source number). However, SS-based methods realize decorrelation at the expense of the reduction in array aperture, which may lead to poor DOA estimation performance. The Spatial Differencing Smoothing based techniques proposed in [10–13] can estimate the uncorrelated and coherent sources separately, which enlarged the effective array aperture accordingly. Rajagopal et al. firstly introduced the spatial differencing technique [10] which has the inherent limitation that the number of coherent sources in one group must be no more than two. Subsequently, an improved spatial differencing method [11] was proposed by taking advantages of both Toeplitz and non-Toeplitz properties of the array covariance matrix to estimate more sources, but this method may fail to work as a result of rank loss on condition that the number of coherent sources in a coherent group is odd. Liu et al. [12] proposed a new spatial differencing method, which can efficiently detect the DOAs of mixed sources no matter the number of coherent sources is even or odd. Ye et al. [13] distinguished the uncorrelated sources from coherent sources by taking advantage of the symmetric property of the ULA. As the power of coherent sources would decrease

* Corresponding author.
E-mail addresses: swj0418@263.net (W. Si), zhaopinjiao@hrbeu.edu.cn (P. Zhao), quzhiyu@hrbeu.edu.cn (Z. Qu), wangyan17855@163.com (Y. Wang).

http://dx.doi.org/10.1016/j.dsp.2016.07.024
1051-2004/

when removing the uncorrelated sources, the spatial differencing-based techniques mentioned above would suffer from the performance deterioration. As a result, the oblique projection technique was utilized in [6,14–17], where the uncorrelated sources can be separated from the coherent sources effectively without power lost. Ye et al. [18], Gan et al. [19] and Shi et al. [20] exploited the moduli of the eigenvalues to distinguish uncorrelated sources from coherent sources, but these methods were accomplished by using several computational intensive complex-valued eigenvalue decomposition (EVD) operations. In view of the fact that the methods in [6–20] involve an amount of complex-valued computations, and even the tremendous spectral search operations [7–15,18–20], they all suffer from heavy computational burden. A sparsity-based DOA estimation method for coherent and uncorrelated targets was investigated in [21], wherein computationally intensive iterative process was required for the DOA estimation. A partial real-valued DOA estimation method referred to as EDE method was proposed in [22], where only the uncorrelated sources were resolved in the real-valued domain and the coherent sources were resolved using multiple complex-valued EVD operations, thus, the computational complexity may still be too high for real-time applications [17]. Some efforts have been made to reduce the computational complexity. The unitary transformation method [23] and its variants [24–28] (referred to as real-valued methods) were developed to convert complex-valued matrices into the corresponding real-valued versions, with which about 3/4 computational load can be reduced. Among these real-valued methods, [24,25,27,28] are applicable for the DOA estimation. Zheng et al. [24] developed a unitary ESPRIT method for the joint direction of departure (DOD) and DOA estimation. Huang et al. [25] developed a real-valued MVDR beamformer for spherical arrays based on the frequency invariant steering matrix. Qian et al. [27] presented a unitary root-MUSIC algorithm by combing the conventional beamforming and unitary root-MUSIC. The literature [28] introduced a real-valued DOA estimation approach for the coherent sources which was referred to as unitary MP. Unfortunately, these real-valued methods are only applicable for either uncorrelated sources [24,25,27] or coherent sources [28]. In addition, another limitation of these real-valued methods is that the number of sensors must be larger than that of sources. Different from the unitary transformation methods, Yan et al. proposed a real-valued MUSIC method [29] by separating the real part from the imaginary part of the array output covariance matrix. However, to the best of our knowledge, the real-valued DOA estimation method under the coexistence of uncorrelated and coherent sources has not been addressed.

To address the issue just mentioned, a novel real-valued DOA estimation (RVDE) method for a mixture of uncorrelated and coherent sources is proposed in this paper. Firstly, an augmented matrix is constructed and then transformed into a real-valued version by exploiting a unitary transformation, which enlarges the effective array aperture. The DOAs of uncorrelated sources are obtained from the EVD of the real-valued augmented matrix, together with a selection criterion. Afterwards, the contributions of the uncorrelated sources are removed via introducing an oblique projection operator, with which only coherent components remain. Then, in order to estimate the DOAs of coherent sources, a real-valued coherent augmented matrix with an extended array aperture is constructed. With the coherent DOA estimates, the fading coefficients are obtained by adding penalties to a constraint quadratic minimization problem. The proposed real-valued DOA estimation method under the coexistence of uncorrelated and coherent sources shows improved estimation accuracy with reduced computational complexity. Another notable advantage of the proposed method is that it can resolve more sources than the number of sensors, which is attributed to the incorporation of augmented matrices. Simulation results show the effectiveness and the favorable performance of the proposed method. Now we briefly summarize the contributions of this work as follows:

i). A real-valued DOA estimation method for a mixture of uncorrelated and coherent sources is proposed by employing the unitary transformation, which has been demonstrated to be computationally efficient.
ii). More sources than the number of sensors can be resolved benefiting from the proposed augmented matrices
iii). The identifiability, computational complexity and theoretical mean square error (MSE) of the proposed method are discussed in detail.
iv). The fading coefficients estimation problem is transformed into a modified constraint quadratic minimization problem by adding penalties, which guarantees the stability of solution.

The mathematical notations used throughout this paper are denoted as follows. Vectors and matrices are denoted by lowercase and uppercase bold-face italic letters, respectively. $\mathbb{C}$ denotes the complex space. $(\cdot)^T$, $(\cdot)^*$, $(\cdot)^H$, $(\cdot)^{-1}$, $(\cdot)^\dagger$, $\otimes$ and $\mathrm{E}[\cdot]$ represent transpose, conjugate, conjugate transpose, inverse, Moore–Penrose inverse, Kronecker product and the statistical expectation, respectively. $\mathbf{0}_{m\times n}$, $\boldsymbol{I}_m$ and $\boldsymbol{J}_m$ represent an $m\times n$ null matrix, an $m\times m$ identity matrix and an $m\times m$ exchange matrix with ones on its antidiagonal and zeros elsewhere, respectively. $\mathrm{Re}(\cdot)$ and $\mathrm{Im}(\cdot)$ indicate the real and the imaginary part of the embraced matrix. Additionally, $\lfloor\cdot\rfloor$ and $\lceil\cdot\rceil$ are the floor and ceil operators, respectively. $\mathrm{rank}(\cdot)$, $\|\cdot\|$, and $\mathrm{span}(\cdot)$ are the rank of the embraced matrix, the Frobenius norm and the column-spaces of the embraced matrix. $\mathrm{diag}\{\cdot\}$ and $\mathrm{blkdiag}\{\cdot\}$ denote a diagonal matrix and a block diagonal matrix, respectively. Furthermore, $\mathrm{var}(\theta_{u_k})$ and $\mathrm{var}(\theta_{c_k})$ denote the theoretical MSE of the DOA estimates of the kth uncorrelated and the kth coherent sources, respectively.

The remainder of paper is organized as follows. The DOA estimation model for mixed sources is formulated in Section 2. Section 3 presents the proposed real-valued DOA estimation method for a mixture of uncorrelated and coherent sources in detail. The identifiability, computational complexity, theoretical MSE and the estimation of fading coefficients of the proposed method are discussed in Section 4. Section 5 exhibits the simulation performance of the proposed method. Conclusions are drawn in Section 6.

2. Problem formulation

Consider a ULA consisting of M omnidirectional sensors with the interspacing between adjacent sensors being d. Assuming that a total of K far-field narrowband sources with the carrier wavelength λ impinge on this ULA, where the first P sources are mutually uncorrelated with the power of each source $s_k(t)$ being $\sigma_k^2, k=1,\cdots,P$, and the remains are the L groups of Q coherent sources owing to the multipath propagation. Among the L groups of coherent sources, the kth group has n_k sources with the complex fading coefficient $\varsigma_{k,n}$, which is engendered from the multipath propagation of the kth source $s_k(t)$ with the power σ_k^2, for $k=P+1,\cdots,P+L$ and $n=1,\cdots,n_k$. Based on the descriptions above, the number of coherent sources can be expressed as $Q=K-P=\sum_{k=P+1}^{P+L} n_{k-P}$. Then the $M\times 1$ array output vector $\boldsymbol{x}(t)$ at time t can be expressed as

$$\begin{aligned}\boldsymbol{x}(t) &= \sum_{k=1}^{P}\boldsymbol{a}(\theta_k)s_k(t)+\sum_{k=P+1}^{P+L}\sum_{n=1}^{n_k}\boldsymbol{a}(\theta_{k,n})\varsigma_{k,n}s_k(t)+\boldsymbol{n}(t)\\ &= \boldsymbol{A}_u\boldsymbol{s}_u(t)+\boldsymbol{A}_c\boldsymbol{\Upsilon}\boldsymbol{s}_c(t)+\boldsymbol{n}(t)\\ &= \boldsymbol{A}\boldsymbol{E}\boldsymbol{s}(t)+\boldsymbol{n}(t),\quad t=1,2,\cdots,N\end{aligned}\tag{1}$$

where N is the number of snapshots. $\boldsymbol{a}(\theta_k) = [1, e^{-j2\pi d \sin\theta_k/\lambda}, \cdots, e^{-j2\pi(M-1)d\sin\theta_k/\lambda}]^T \in \mathbb{C}^M$ represents the $M \times 1$ steering vector corresponding to the direction θ_k, and $\boldsymbol{n}(t)$ is the $M \times 1$ noise vector with the power σ_n^2. The array manifold matrix $\boldsymbol{A}$ is defined by $\boldsymbol{A} = [\boldsymbol{A}_u, \boldsymbol{A}_c] \in \mathbb{C}^{M\times K}$, in which $\boldsymbol{A}_u = [\boldsymbol{a}(\theta_1), \boldsymbol{a}(\theta_2), \cdots, \boldsymbol{a}(\theta_P)] \in \mathbb{C}^{M\times P}$ and $\boldsymbol{A}_c = [\boldsymbol{A}_{c,P+1}, \boldsymbol{A}_{c,P+2}, \cdots, \boldsymbol{A}_{c,P+L}] \in \mathbb{C}^{M\times Q}$ are corresponding to the P uncorrelated sources and Q coherent sources, respectively with $\boldsymbol{A}_{c,k} = [\boldsymbol{a}(\theta_{k,1}), \boldsymbol{a}(\theta_{k,2}), \cdots, \boldsymbol{a}(\theta_{k,n_k})] \in \mathbb{C}^{M\times n_k}$ being the array manifold matrix of the kth group coherent sources. $\boldsymbol{s}(t) = [\boldsymbol{s}_u^T(t), \boldsymbol{s}_c^T(t)]^T \in \mathbb{C}^{(P+L)}$ is the source vector. $\boldsymbol{s}_u(t) = [s_1(t), s_2(t), \cdots, s_P(t)]^T \in \mathbb{C}^P$ and $\boldsymbol{s}_c(t) = [s_{P+1}(t), s_{P+2}(t), \cdots, s_{P+L}(t)]^T \in \mathbb{C}^L$ represent the uncorrelated and coherent source vector, respectively. $\boldsymbol{\Upsilon} = \text{blkdiag}\{\boldsymbol{\varsigma}_{P+1}, \boldsymbol{\varsigma}_{P+2}, \cdots, \boldsymbol{\varsigma}_{P+L}\} \in \mathbb{C}^{Q\times L}$ is the fading coefficient matrix whose column vector can be expressed as $\boldsymbol{\varsigma}_k = [\varsigma_{k,1}, \varsigma_{k,2}, \cdots, \varsigma_{k,n_k}]^T \in \mathbb{C}^{n_k}$. For the convenience of analysis, we define a $K \times (P+L)$ matrix as $\boldsymbol{E} = \text{blkdiag}\{\boldsymbol{I}_P, \boldsymbol{\Upsilon}\}$.

The basic assumptions utilized throughout this paper are listed as follows.

(A1) $\boldsymbol{s}(t)$ and $\boldsymbol{n}(t)$ are the zero-mean stationary Gaussian random processes, and the entries of $\boldsymbol{n}(t)$ are uncorrelated with each other, as well as $\boldsymbol{s}(t)$.

(A2) The coherent sources in different groups are from L statistically independent sources $s_{P+1}(t), \cdots, s_{P+L}(t)$, thus they are uncorrelated with each other. Besides, they are uncorrelated with the first P uncorrelated sources $s_1(t), \cdots, s_P(t)$.

(A3) The number of uncorrelated sources, coherent sources, coherent groups (i.e., the values of P, Q, L) can be estimated by the source number estimation methods (cf. [30]).

(A4) Due to the fading coefficients are slowly varying, they are thought to be unchanged during the DOA estimation processing. Moreover, the first source in each coherent group is assumed to be the smallest DOA with the corresponding fading coefficient being normalized to unity (cf. [31]).

Under the above assumptions, an augmented matrix is constructed as

$$\tilde{\boldsymbol{X}} = \begin{bmatrix} \boldsymbol{X} \\ \boldsymbol{J}_M \boldsymbol{X}^* \boldsymbol{J}_N \end{bmatrix} = \begin{bmatrix} \boldsymbol{A}_u \boldsymbol{S}_u \\ \boldsymbol{J}_M \boldsymbol{A}_u^* \boldsymbol{S}_u^* \boldsymbol{J}_N \end{bmatrix} + \begin{bmatrix} \boldsymbol{A}_c \boldsymbol{\Upsilon} \boldsymbol{S}_c \\ \boldsymbol{J}_M \boldsymbol{A}_c^* \boldsymbol{\Upsilon}^* \boldsymbol{S}_c^* \boldsymbol{J}_N \end{bmatrix} + \begin{bmatrix} \boldsymbol{N} \\ \boldsymbol{J}_M \boldsymbol{N}^* \boldsymbol{J}_N \end{bmatrix} \tag{2}$$

where $\boldsymbol{X} = [\boldsymbol{x}(1), \boldsymbol{x}(2), \cdots, \boldsymbol{x}(N)]$, $\boldsymbol{N} = [\boldsymbol{n}(1), \boldsymbol{n}(2), \cdots, \boldsymbol{n}(N)]$, $\boldsymbol{S}_u = [\boldsymbol{s}_u(1), \boldsymbol{s}_u(2), \cdots, \boldsymbol{s}_u(N)]$ and $\boldsymbol{S}_c = [\boldsymbol{s}_c(1), \boldsymbol{s}_c(2), \cdots, \boldsymbol{s}_c(N)]$. $\tilde{\boldsymbol{X}}$ is a $2M \times N$ centro-Hermitian matrix that satisfies $\tilde{\boldsymbol{X}} = \boldsymbol{J}_{2M} \tilde{\boldsymbol{X}}^* \boldsymbol{J}_N$. Since $\boldsymbol{A}_u$ and $\boldsymbol{A}_c$ are Vandermonde matrices, the equalities $\boldsymbol{J}_M \boldsymbol{A}_u^* = \boldsymbol{A}_u \boldsymbol{\Delta}_u$ and $\boldsymbol{J}_M \boldsymbol{A}_c^* = \boldsymbol{A}_c \boldsymbol{\Delta}_c$ hold respectively with $\boldsymbol{\Delta}_u = \text{diag}\{e^{-j2\pi d \sin\theta_1/\lambda}, e^{-j2\pi d \sin\theta_2/\lambda}, \cdots, e^{-j2\pi d \sin\theta_P/\lambda}\} \in \mathbb{C}^{P\times P}$ and $\boldsymbol{\Delta}_c = \text{diag}\{e^{-j2\pi d \sin\theta_{P+1,1}/\lambda}, \cdots, e^{-j2\pi d \sin\theta_{P+1,n_1}/\lambda}, \cdots, e^{-j2\pi d \sin\theta_{P+L,1}/\lambda}, \cdots, e^{-j2\pi d \sin\theta_{P+L,n_L}/\lambda}\} \in \mathbb{C}^{Q\times Q}$. Note that the row number of the augmented matrix $\tilde{\boldsymbol{X}}$ is twice of that of the original matrix $\boldsymbol{X}$, namely, the augmented arrays have M virtual sensors more than the original ULA, which can help to resolve more sources.

According to the above analysis, we have

$$\begin{aligned} \tilde{\boldsymbol{X}} &= \begin{bmatrix} \boldsymbol{A}_u \boldsymbol{S}_u \\ \boldsymbol{A}_u \boldsymbol{\Delta}_u \boldsymbol{S}_u^* \boldsymbol{J}_N \end{bmatrix} + \begin{bmatrix} \boldsymbol{A}_c \boldsymbol{\Upsilon} \boldsymbol{S}_c \\ \boldsymbol{A}_c \boldsymbol{\Delta}_c \boldsymbol{\Upsilon}^* \boldsymbol{S}_c^* \boldsymbol{J}_N \end{bmatrix} + \begin{bmatrix} \boldsymbol{N} \\ \boldsymbol{J}_M \boldsymbol{N}^* \boldsymbol{J}_N \end{bmatrix} \\ &= \tilde{\boldsymbol{A}}_u \tilde{\boldsymbol{S}}_u + \tilde{\boldsymbol{A}}_c \tilde{\boldsymbol{S}}_c + \tilde{\boldsymbol{N}} = \tilde{\boldsymbol{A}} \tilde{\boldsymbol{S}} + \tilde{\boldsymbol{N}} \end{aligned} \tag{3}$$

with $\tilde{\boldsymbol{A}}_u = \boldsymbol{I}_2 \otimes \boldsymbol{A}_u$, $\tilde{\boldsymbol{A}}_c = \boldsymbol{I}_2 \otimes \boldsymbol{A}_c$, $\tilde{\boldsymbol{S}}_u = \begin{bmatrix} \boldsymbol{S}_u \\ \boldsymbol{\Delta}_u \boldsymbol{S}_u^* \boldsymbol{J}_N \end{bmatrix}$, $\tilde{\boldsymbol{S}}_c = \begin{bmatrix} \boldsymbol{\Upsilon} \boldsymbol{S}_c \\ \boldsymbol{\Delta}_c \boldsymbol{\Upsilon}^* \boldsymbol{S}_c^* \boldsymbol{J}_N \end{bmatrix}$ and $\tilde{\boldsymbol{N}} = \begin{bmatrix} \boldsymbol{N} \\ \boldsymbol{J}_M \boldsymbol{N}^* \boldsymbol{J}_N \end{bmatrix}$. According to [24], a unitary transformation can map a centro-Hermitian matrix to a real-valued matrix, hence a real-valued matrix $\hat{\boldsymbol{X}}$ is constructed as follows

$$\begin{aligned} \hat{\boldsymbol{X}} = \boldsymbol{Q}_{2M}^H \tilde{\boldsymbol{X}} \boldsymbol{Q}_N &= \boldsymbol{Q}_{2M}^H \tilde{\boldsymbol{A}}_u \tilde{\boldsymbol{S}}_u \boldsymbol{Q}_N + \boldsymbol{Q}_{2M}^H \tilde{\boldsymbol{A}}_c \tilde{\boldsymbol{S}}_c \boldsymbol{Q}_N \\ &\quad + \boldsymbol{Q}_{2M}^H \tilde{\boldsymbol{N}} \boldsymbol{Q}_N \end{aligned} \tag{4}$$

where $\boldsymbol{Q}_m = \frac{1}{\sqrt{2}} \begin{bmatrix} \boldsymbol{I}_{\frac{m-1}{2}} & \boldsymbol{0} & j\boldsymbol{I}_{\frac{m-1}{2}} \\ \boldsymbol{0}^T & \sqrt{2} & \boldsymbol{0}^T \\ \boldsymbol{\Pi}_{\frac{m-1}{2}} & \boldsymbol{0} & -j\boldsymbol{\Pi}_{\frac{m-1}{2}} \end{bmatrix}$ if m is odd, and a $\boldsymbol{Q}_m$ of even order is obtained by casting out the center row and center column of the $\boldsymbol{Q}_m$ of odd order.

The covariance matrix of the real-valued matrix $\hat{\boldsymbol{X}}$ with the size $2M \times 2M$ is expressed as

$$\begin{aligned} \hat{\boldsymbol{R}} = E\big[\hat{\boldsymbol{X}}\hat{\boldsymbol{X}}^H\big] &= \boldsymbol{Q}_{2M}^H \tilde{\boldsymbol{A}}_u \tilde{\boldsymbol{R}}_{s_u} \tilde{\boldsymbol{A}}_u^H \boldsymbol{Q}_{2M} \\ &\quad + \boldsymbol{Q}_{2M}^H \tilde{\boldsymbol{A}}_c \tilde{\boldsymbol{R}}_{s_c} \tilde{\boldsymbol{A}}_c^H \boldsymbol{Q}_{2M} + \boldsymbol{Q}_{2M}^H \tilde{\boldsymbol{R}}_n \boldsymbol{Q}_{2M} \\ &= \hat{\boldsymbol{A}}_u \tilde{\boldsymbol{R}}_{s_u} \hat{\boldsymbol{A}}_u^H + \hat{\boldsymbol{A}}_c \tilde{\boldsymbol{R}}_{s_c} \hat{\boldsymbol{A}}_c^H + \hat{\boldsymbol{R}}_n \end{aligned} \tag{5}$$

where $\hat{\boldsymbol{A}}_u = \boldsymbol{Q}_{2M}^H (\boldsymbol{I}_2 \otimes \boldsymbol{A}_u)$ and $\hat{\boldsymbol{A}}_c = \boldsymbol{Q}_{2M}^H (\boldsymbol{I}_2 \otimes \boldsymbol{A}_c)$. Denote the array manifold matrix of real-valued matrix $\hat{\boldsymbol{X}}$ as $\hat{\boldsymbol{A}} = [\hat{\boldsymbol{A}}_u, \hat{\boldsymbol{A}}_c]$, and $\hat{\boldsymbol{A}}$ can also be expressed as $\hat{\boldsymbol{A}} = \boldsymbol{Q}_{2M}^H (\boldsymbol{I}_2 \otimes \boldsymbol{A})$. In addition, $\tilde{\boldsymbol{R}}_{s_u} = E[\tilde{\boldsymbol{S}}_u \tilde{\boldsymbol{S}}_u^H]$, $\tilde{\boldsymbol{R}}_{s_c} = E[\tilde{\boldsymbol{S}}_c \tilde{\boldsymbol{S}}_c^H]$ and $\tilde{\boldsymbol{R}}_n = E[\tilde{\boldsymbol{N}} \tilde{\boldsymbol{N}}^H]$ are the augmented covariance matrices with respect to $\tilde{\boldsymbol{S}}_u$, $\tilde{\boldsymbol{S}}_c$ and $\tilde{\boldsymbol{N}}$, respectively.

3. The real-valued DOA estimation

In this section, a real-valued DOA estimation (RVDE) method for a mixture of uncorrelated and coherent sources is elaborated. Both the uncorrelated and coherent sources are estimated via real-valued calculations without computationally expensive operations, such as spectral search and iterative process. Besides, the effective array aperture is enlarged by constructing augmented matrices, so that more sources than the number of sensors are able to be resolved.

3.1. DOA estimation of uncorrelated sources

In the complex-valued domain, array manifold matrix $\boldsymbol{A}$ satisfies the rotational invariance, i.e., $\boldsymbol{K}_2^{M-1} \boldsymbol{A} = \boldsymbol{K}_1^{M-1} \boldsymbol{A} \boldsymbol{\Phi}$, where $\boldsymbol{K}_1^m$ and $\boldsymbol{K}_2^m$ are two $m \times (m+1)$ selection matrices defined as $\boldsymbol{K}_1^m = [\boldsymbol{I}_m, \boldsymbol{0}_{m\times 1}]_{m\times(m+1)}$ and $\boldsymbol{K}_2^m = [\boldsymbol{0}_{m\times 1}, \boldsymbol{I}_m]_{m\times(m+1)}$ respectively, and $\boldsymbol{\Phi} = \text{blkdiag}\{\boldsymbol{\Delta}_u, \boldsymbol{\Delta}_c\}$ is a $K \times K$ diagonal matrix containing the DOA information of both uncorrelated and coherent sources. Rewrite the rotational invariance, we have

$$\big(\boldsymbol{I}_2 \otimes \boldsymbol{K}_2^{M-1}\big)(\boldsymbol{I}_2 \otimes \boldsymbol{A}) = \big(\boldsymbol{I}_2 \otimes \boldsymbol{K}_1^{M-1}\big)(\boldsymbol{I}_2 \otimes \boldsymbol{A})\boldsymbol{\Psi} \tag{6}$$

where $\boldsymbol{\Psi} = \boldsymbol{I}_2 \otimes \boldsymbol{\Phi}$ is a $2K \times 2K$ diagonal matrix. Based on the definition of $\hat{\boldsymbol{A}}$, (6) can be further expressed as

$$\boldsymbol{Q}_{2M-2}^H \big(\boldsymbol{I}_2 \otimes \boldsymbol{K}_2^{M-1}\big) \boldsymbol{Q}_{2M} \hat{\boldsymbol{A}} = \boldsymbol{Q}_{2M-2}^H \big(\boldsymbol{I}_2 \otimes \boldsymbol{K}_1^{M-1}\big) \boldsymbol{Q}_{2M} \hat{\boldsymbol{A}} \boldsymbol{\Psi} \tag{7}$$

Note that (7) is the real-valued form of the rotational invariance, and it is easy to see that $\boldsymbol{Q}_{2M-2}^H (\boldsymbol{I}_2 \otimes \boldsymbol{K}_2^{M-1}) \boldsymbol{Q}_{2M} = (\boldsymbol{Q}_{2M-2}^H (\boldsymbol{I}_2 \otimes \boldsymbol{K}_1^{M-1}) \boldsymbol{Q}_{2M})^*$ holds. By defining two real-valued matrices

$$\begin{aligned} \boldsymbol{P}_1 &= \boldsymbol{Q}_{2M-2}^H \big(\big(\boldsymbol{I}_2 \otimes \boldsymbol{K}_1^{M-1}\big) + \big(\boldsymbol{I}_2 \otimes \boldsymbol{K}_2^{M-1}\big)\big) \boldsymbol{Q}_{2M} \\ &= 2\,\text{Re}\big\{ \boldsymbol{Q}_{2M-2}^H \big(\boldsymbol{I}_2 \otimes \boldsymbol{K}_2^{M-1}\big) \boldsymbol{Q}_{2M} \big\} \end{aligned} \tag{8}$$

$$\begin{aligned} \boldsymbol{P}_2 &= \boldsymbol{Q}_{2M-2}^H j\big(\big(\boldsymbol{I}_2 \otimes \boldsymbol{K}_1^{M-1}\big) - \big(\boldsymbol{I}_2 \otimes \boldsymbol{K}_2^{M-1}\big)\big) \boldsymbol{Q}_{2M} \\ &= 2\,\text{Im}\big\{ \boldsymbol{Q}_{2M-2}^H \big(\boldsymbol{I}_2 \otimes \boldsymbol{K}_2^{M-1}\big) \boldsymbol{Q}_{2M} \big\}, \end{aligned} \tag{9}$$

the real-valued form of equation (7) can be rewritten as

$$(\boldsymbol{P}_1 + j\boldsymbol{P}_2)\hat{\boldsymbol{A}} = (\boldsymbol{P}_1 - j\boldsymbol{P}_2)\hat{\boldsymbol{A}}\boldsymbol{\Psi} \tag{10}$$

By further derivation, (10) can be simplified to

$$\boldsymbol{P}_2\hat{\boldsymbol{A}} = \boldsymbol{P}_1\hat{\boldsymbol{A}}\boldsymbol{\Omega} \tag{11}$$

where $\boldsymbol{\Omega} = -j(\boldsymbol{\Psi}-\boldsymbol{I})(\boldsymbol{\Psi}+\boldsymbol{I})^{-1}$ holds, and the matrix $\boldsymbol{\Omega}$ that contains the angular information of incident sources can be calculated by

$$\begin{aligned}\boldsymbol{\Omega} &= (\boldsymbol{P}_1\hat{\boldsymbol{A}})^{\dagger}(\boldsymbol{P}_2\hat{\boldsymbol{A}}) \\ &= \left(\boldsymbol{Q}_{2M-2}^{H}\left(\boldsymbol{I}_2\otimes\left(\boldsymbol{K}_1^{M-1}+\boldsymbol{K}_2^{M-1}\right)\right)\boldsymbol{Q}_{2M}\boldsymbol{Q}_{2M}^{H}(\boldsymbol{I}_2\otimes\boldsymbol{A})\right)^{\dagger} \\ &\quad\times\left(\boldsymbol{Q}_{2M-2}^{H}j\left(\boldsymbol{I}_2\otimes\left(\boldsymbol{K}_1^{M-1}-\boldsymbol{K}_2^{M-1}\right)\right)\boldsymbol{Q}_{2M}\boldsymbol{Q}_{2M}^{H}(\boldsymbol{I}_2\otimes\boldsymbol{A})\right) \\ &= \boldsymbol{I}_2\otimes\begin{bmatrix} j\boldsymbol{\Theta}_{u-}\boldsymbol{\Theta}_{u+}^{-1} & \boldsymbol{F}_1 \\ \boldsymbol{0}_{L\times P} & \boldsymbol{F}_2\end{bmatrix}\end{aligned} \tag{12}$$

where

$$\begin{bmatrix}\boldsymbol{F}_1\\ \boldsymbol{F}_2\end{bmatrix} = j\begin{bmatrix}\boldsymbol{\Theta}_{u+}^{H}\boldsymbol{A}_{u1}^{H}\boldsymbol{A}_{u1}\boldsymbol{\Theta}_{u+} & \boldsymbol{\Theta}_{u+}^{H}\boldsymbol{A}_{u1}^{H}\boldsymbol{A}_{c1}\boldsymbol{\Theta}_{c+}\boldsymbol{\Upsilon} \\ \boldsymbol{\Upsilon}^{H}\boldsymbol{\Theta}_{c+}^{H}\boldsymbol{A}_{c1}^{H}\boldsymbol{A}_{u1}\boldsymbol{\Theta}_{u+} & \boldsymbol{\Upsilon}^{H}\boldsymbol{\Theta}_{c+}^{H}\boldsymbol{A}_{c1}^{H}\boldsymbol{A}_{c1}\boldsymbol{\Theta}_{c+}\boldsymbol{\Upsilon}\end{bmatrix}^{-1} \times\begin{bmatrix}\boldsymbol{\Theta}_{u+}^{H}\boldsymbol{A}_{u1}^{H}\boldsymbol{A}_{c1}\boldsymbol{\Theta}_{c-}\boldsymbol{\Upsilon} \\ \boldsymbol{\Upsilon}^{H}\boldsymbol{\Theta}_{c+}^{H}\boldsymbol{A}_{c1}^{H}\boldsymbol{A}_{c1}\boldsymbol{\Theta}_{c-}\boldsymbol{\Upsilon}\end{bmatrix},$$

and $\boldsymbol{A}_{u1}$ and $\boldsymbol{A}_{c1}$ denote the first $M-1$ rows of $\boldsymbol{A}_u$ and $\boldsymbol{A}_c$, respectively (cf. [22]). For notational convenience, we define $\boldsymbol{\Theta}_{u+} = \boldsymbol{I}_P+\boldsymbol{\Delta}_u$, $\boldsymbol{\Theta}_{u-} = \boldsymbol{I}_P-\boldsymbol{\Delta}_u$, $\boldsymbol{\Theta}_{c+} = \boldsymbol{I}_Q+\boldsymbol{\Delta}_c$ and $\boldsymbol{\Theta}_{c-} = \boldsymbol{I}_Q-\boldsymbol{\Delta}_c$ (see Appendix A for details).

Performing EVD on $\hat{\boldsymbol{R}}$, we have

$$\hat{\boldsymbol{R}} = \boldsymbol{E}_s\boldsymbol{\Sigma}_s\boldsymbol{E}_s^{T}+\boldsymbol{E}_n\boldsymbol{\Sigma}_n\boldsymbol{E}_n^{T} \tag{13}$$

where $\boldsymbol{E}_s$ and $\boldsymbol{E}_n$ are the real-valued eigenvector matrices corresponding to source and noise subspace, respectively. $\boldsymbol{\Sigma}_s$ is a real-valued eigenvalue matrix that composes of the $2(P+L)$ large eigenvalues, while $\boldsymbol{\Sigma}_n$ is composed of the $2(M-P-L)$ small eigenvalues. Since the columns of $\boldsymbol{E}_s$ span the real-valued source subspace that is spanned by the columns of $\hat{\boldsymbol{A}}$ as well, i.e., $\mathrm{span}(\boldsymbol{E}_s) = \mathrm{span}(\hat{\boldsymbol{A}})$, there must exist a $2(P+L)\times 2(P+L)$ full rank matrix $\boldsymbol{T}_s$ that satisfies $\boldsymbol{E}_s = \hat{\boldsymbol{A}}\boldsymbol{T}_s$. For practical situations, the calculation of $\hat{\boldsymbol{A}}$ is commonly unavailable, and the associated source subspace $\boldsymbol{E}_s$ is usually used for substitution.

Thus, rewrite (11) as

$$\boldsymbol{P}_2\boldsymbol{E}_s = \boldsymbol{P}_1\boldsymbol{E}_s\tilde{\boldsymbol{\Omega}} \tag{14}$$

where $\tilde{\boldsymbol{\Omega}} = \boldsymbol{T}_s^{-1}\boldsymbol{\Omega}\boldsymbol{T}_s$. Obviously, $\boldsymbol{\Omega}$ is a diagonal matrix which has the same eigenvalues with $\tilde{\boldsymbol{\Omega}}$.

Combining (12) and (14) yields

$$\tilde{\boldsymbol{\Omega}} = \boldsymbol{T}_s^{-1}\left(\boldsymbol{I}_2\otimes\begin{bmatrix} j\boldsymbol{\Theta}_{u-}\boldsymbol{\Theta}_{u+}^{-1} & \boldsymbol{F}_1 \\ \boldsymbol{0}_{L\times P} & \boldsymbol{F}_2\end{bmatrix}\right)\boldsymbol{T}_s \tag{15}$$

It can be implied that the DOAs of uncorrelated sources can be resolved by performing EVD on $\tilde{\boldsymbol{\Omega}}$, since $j\boldsymbol{\Theta}_{u-}\boldsymbol{\Theta}_{u+}^{-1}$ is a diagonal matrix consisting of DOA information of uncorrelated sources with the kth element being $\tan(\pi d\sin\theta_k/\lambda)$ for $k=1,\cdots,P$. Due to the fact that the rank of $\tilde{\boldsymbol{\Omega}}$ is $2(P+L)$, the $2(P+L)$ nonzero eigenvalues $\eta_1,\eta_2,\cdots,\eta_{2(P+L)}$ are used for the DOA estimation of uncorrelated sources, i.e.,

$$\hat{\theta}_{u_k} = \arcsin\left(\frac{\lambda}{\pi d}\arctan(\eta_k)\right),\quad k=1,2,\cdots,2(P+L) \tag{16}$$

However, there will be $P+2L$ erroneous estimates along with P true estimates corresponding to P uncorrelated sources. The reason is that the rank of $\hat{\boldsymbol{A}}$ is doubled compared with that of $\boldsymbol{A}$, i.e., $\mathrm{rank}(\hat{\boldsymbol{A}}) = 2\,\mathrm{rank}(\boldsymbol{A})$. Thus, a selection criterion that distinguishes P correct estimates from $P+2L$ erroneous estimates is presented by calculating $h_k = \|\boldsymbol{a}^{H}(\hat{\theta}_{u_k})\boldsymbol{V}_n\|$, where $\boldsymbol{V}_n$ is the noise subspace spanned by the left singular vector matrix corresponding to the $M-P-L$ small singular values of $\boldsymbol{x}(t)$. It is clear that the steering vector $\boldsymbol{a}(\hat{\theta}_{u_k})$ is orthogonal to the noise subspace $\boldsymbol{V}_n$ (i.e., in the noise corrupted situations, $h_k\approx 0$ holds) only if $\hat{\theta}_{u_k}$ belongs to one of the uncorrelated incident sources. Therefore, P true DOAs that corresponding to P uncorrelated sources are selected from $2(P+L)$ candidate angles.

As compared with the EDE method mentioned in [22], the proposed RVDE method can resolve more uncorrelated sources by exploiting the augmented matrix of direct received data. Moreover, the DOA estimation for the coherent sources is also calculated in the real-valued domain, while the EDE method realizes the coherent DOA estimation via the complex-valued computations (see Section 3.2 for details).

3.2. DOA estimation of coherent sources

Most existing DOA estimation methods for coherent sources are implemented in the complex-valued domain with a heavy computational load, thus they may not be suitable for real-time applications. To reduce the computational burden and resolve more sources, we present an extension matrix, referred to as the real-valued coherent augmented matrix (CA-matrix). The contributions of the estimated uncorrelated sources should be excluded at first. Following from [15], an oblique projection operator is formulated as

$$\boldsymbol{C} = \bar{\boldsymbol{A}}_u\left(\bar{\boldsymbol{A}}_u^{H}\bar{\boldsymbol{R}}^{-1}\bar{\boldsymbol{A}}_u\right)^{-1}\bar{\boldsymbol{A}}_u^{H}\bar{\boldsymbol{R}}^{-1} \tag{17}$$

where $\bar{\boldsymbol{A}}_u = [\boldsymbol{a}(\hat{\theta}_{u_1}),\boldsymbol{a}(\hat{\theta}_{u_2}),\cdots,\boldsymbol{a}(\hat{\theta}_{u_P})]$ is the reconstructed array manifold matrix of the estimated uncorrelated sources. $\bar{\boldsymbol{R}}$ is the covariance matrix with noise term cancellation, and it can be calculated by $\bar{\boldsymbol{R}} = E[\boldsymbol{X}\boldsymbol{X}^{H}]-\sigma_n^2\boldsymbol{I}_M = \boldsymbol{A}_u\boldsymbol{R}_u\boldsymbol{A}_u^{H}+\boldsymbol{A}_c\boldsymbol{\Upsilon}\boldsymbol{R}_c\boldsymbol{\Upsilon}^{H}\boldsymbol{A}_c^{H}$. By exploiting the property of oblique projection [16], only the coherent components are retained in $\hat{\boldsymbol{R}}_c$ as

$$\hat{\boldsymbol{R}}_c = (\boldsymbol{I}_M-\boldsymbol{C})\bar{\boldsymbol{R}}(\boldsymbol{I}_M-\boldsymbol{C})^{H} = \boldsymbol{A}_c\boldsymbol{\Upsilon}\boldsymbol{R}_c\boldsymbol{\Upsilon}^{H}\boldsymbol{A}_c^{H} \tag{18}$$

where $\hat{\boldsymbol{R}}_c$ is an $M\times M$ matrix and its the (m,n)th element can be given by

$$\hat{\boldsymbol{R}}_c(m,n) = \sum_{l=P+1}^{P+L}\sum_{k=1}^{n_{l-P}} g_{l,k}(m)\mu_{l,k}^{n-1} \tag{19}$$

where $\mu_{l,k} = e^{-j2\pi d\sin\theta_{l,k}/\lambda}$ is the $\sum_{i=1}^{l-P-1}n_i+k$th diagonal element of $\boldsymbol{\Delta}_c$, referred to as the response coefficient of the kth source in the lth coherent group, and

$$g_{l,k}(m) = \sigma_l^2\varsigma_{l,k}^{*}\sum_{d=1}^{n_{l-P}}\varsigma_{l,d}\mu_{l,d}^{1-m} \tag{20}$$

Afterwards, an $(M-G+1)\times G$ matrix is constructed as

$$\boldsymbol{Z}(\bar{m}) = \begin{bmatrix}\hat{\boldsymbol{R}}_c(\bar{m},1) & \hat{\boldsymbol{R}}_c(\bar{m},2) & \cdots & \hat{\boldsymbol{R}}_c(\bar{m},G) \\ \hat{\boldsymbol{R}}_c(\bar{m},2) & \hat{\boldsymbol{R}}_c(\bar{m},3) & \cdots & \hat{\boldsymbol{R}}_c(\bar{m},G+1) \\ \vdots & \vdots & \ddots & \vdots \\ \hat{\boldsymbol{R}}_c(\bar{m},M-G+1) & \hat{\boldsymbol{R}}_c(\bar{m},M-G+2) & \cdots & \hat{\boldsymbol{R}}_c(\bar{m},M)\end{bmatrix}_{(M-G+1)\times G} \tag{21}$$

where the three inequalities $M-G+1>Q$, $G>Q$ and $M/3\le G\le M/2$ must be satisfied.

Combining (19) and (20) yields

$$\boldsymbol{Z}(\bar{m}) = \begin{bmatrix} \sum_{l=P+1}^{P+L}\sum_{k=1}^{n_{l-P}} g_{l,k}(\bar{m}) & \sum_{l=P+1}^{P+L}\sum_{k=1}^{n_{l-P}} g_{l,k}(\bar{m})\mu_{l,k} & \cdots & \sum_{l=P+1}^{P+L}\sum_{k=1}^{n_{l-P}} g_{l,k}(\bar{m})\mu_{l,k}^{G-1} \\ \sum_{l=P+1}^{P+L}\sum_{k=1}^{n_{l-P}} g_{l,k}(\bar{m})\mu_{l,k}^{1} & \sum_{l=P+1}^{P+L}\sum_{k=1}^{n_{l-P}} g_{l,k}(\bar{m})\mu_{l,k}^{2} & \cdots & \sum_{l=P+1}^{P+L}\sum_{k=1}^{n_{l-P}} g_{l,k}(\bar{m})\mu_{l,k}^{G} \\ \vdots & \vdots & \ddots & \vdots \\ \sum_{l=P+1}^{P+L}\sum_{k=1}^{n_{l-P}} g_{l,k}(\bar{m})\mu_{l,k}^{M-G} & \sum_{l=P+1}^{P+L}\sum_{k=1}^{n_{l-P}} g_{l,k}(\bar{m})\mu_{l,k}^{M-G+1} & \cdots & \sum_{l=P+1}^{P+L}\sum_{k=1}^{n_{l-P}} g_{l,k}(\bar{m})\mu_{l,k}^{M-1} \end{bmatrix}_{(M-G+1)\times G}$$
$$= \boldsymbol{Z}_{\mu_1}\boldsymbol{Z}_g\boldsymbol{Z}_{\mu_2} \tag{22}$$

where $\boldsymbol{Z}_{\mu_1}$, $\boldsymbol{Z}_{\mu_2}$ and $\boldsymbol{Z}_g$ are defined as follows

$$\boldsymbol{Z}_{\mu_1} = \big[\boldsymbol{\mu}_{P+1,1}^{(M-G)}, \cdots, \boldsymbol{\mu}_{P+1,n_1}^{(M-G)}, \boldsymbol{\mu}_{P+2,1}^{(M-G)}, \cdots, \boldsymbol{\mu}_{P+2,n_2}^{(M-G)}, \cdots, \boldsymbol{\mu}_{P+L,1}^{(M-G)}, \cdots, \boldsymbol{\mu}_{P+L,n_L}^{(M-G)}\big]_{(M-G+1)\times Q} \tag{23}$$

$$\boldsymbol{Z}_{\mu_2} = \big[\boldsymbol{\mu}_{P+1,1}^{(G-1)}, \cdots, \boldsymbol{\mu}_{P+1,n_1}^{(G-1)}, \boldsymbol{\mu}_{P+2,1}^{(G-1)}, \cdots, \boldsymbol{\mu}_{P+2,n_2}^{(G-1)}, \cdots, \boldsymbol{\mu}_{P+L,1}^{(G-1)}, \cdots, \boldsymbol{\mu}_{P+L,n_L}^{(G-1)}\big]_{Q\times G}^{T} \tag{24}$$

$$\boldsymbol{Z}_g = \operatorname{diag}\big\{g_{P+1,1}(\bar{m}), \cdots, g_{P+1,n_1}(\bar{m}), g_{P+2,1}(\bar{m}), \cdots, g_{P+2,n_2}(\bar{m}), g_{P+L,1}(\bar{m}), \cdots, g_{P+L,n_L}(\bar{m})\big\} \tag{25}$$

where $\boldsymbol{\mu}_{l,k}^{(i)} = [1, \mu_{l,k}^1, \cdots, \mu_{l,k}^i]^T (l = P+1, P+2, \cdots, P+L, k = 1, 2, \cdots, n_{l-P})$. From (22), it is not difficult to prove that the rank of $\boldsymbol{Z}(\bar{m})$ is equal to that of $\boldsymbol{Z}_g$ only if the two equalities $M-G+1 > Q$ and $G > Q$ hold simultaneously. From this, it follows that $\boldsymbol{Z}_g \in \mathbb{C}^{Q\times Q}$ is a full-rank diagonal matrix, and $\boldsymbol{Z}(\bar{m})$ is a full-rank matrix (i.e., $\operatorname{rank}(\boldsymbol{Z}(\bar{m})) = Q$) accordingly. However, the rank of $\boldsymbol{Z}(\bar{m})$ limits the number of resolvable sources, that is, if the matrix $\boldsymbol{Z}(\bar{m})$ is used directly for DOA estimation, at most $\lfloor\frac{M+1}{2}\rfloor$ coherent sources can be resolved from M sensors. In order to estimate more sources, a new matrix $\boldsymbol{B}$, referred to as the coherent augmented matrix (CA-matrix) is defined as

$$\boldsymbol{B} = \big[\boldsymbol{Z}(\bar{m}), \boldsymbol{Z}(\bar{m})\boldsymbol{J}_G, \boldsymbol{J}_{M-G+1}\boldsymbol{Z}^*(\bar{m}), \boldsymbol{J}_{M-G+1}\boldsymbol{Z}^*(\bar{m})\boldsymbol{J}_G\big] \tag{26}$$

where $\boldsymbol{B}$ is a centro-Hermitian matrix (see Appendix B for details), and its column number is four times of the size of $\boldsymbol{Z}(\bar{m})$. With the utilization of $\boldsymbol{B}$, the maximal number of coherent sources that can be resolved increases to $\lfloor\frac{4(M+1)}{5}\rfloor$, as compared with the utilization of $\boldsymbol{Z}(\bar{m})$. Following the similar manner as mentioned in Section 3.1, the CA-matrix $\boldsymbol{B}$ can be transformed into a real-valued matrix as

$$\hat{\boldsymbol{B}} = \boldsymbol{Q}_{M-G+1}^H \boldsymbol{B} \boldsymbol{Q}_{4G} \tag{27}$$

Referring to the MP method [28], we have

$$\tan\frac{\boldsymbol{\Phi}_c}{2} = \chi\Big(\big(\operatorname{Re}\big\{\boldsymbol{Q}_{M-G}^H \boldsymbol{K}_1^{M-G} \boldsymbol{Q}_{M-G+1}\big\}\hat{\boldsymbol{B}}\big)^{\dagger} \times \big(\operatorname{Im}\big\{\boldsymbol{Q}_{M-G}^H \boldsymbol{K}_1^{M-G} \boldsymbol{Q}_{M-G+1}\big\}\hat{\boldsymbol{B}}\big)\Big) \tag{28}$$

where $\chi(\cdot)$ is a eigenvalue operator and $\boldsymbol{\Phi}_c$ represents a set composed of angle information of coherent sources. In the proposed RVDE method, the matrix $\boldsymbol{Z}(\bar{m})$ is constructed from the covariance matrix elements $\hat{\boldsymbol{R}}_c(\bar{m}, n)$ instead of each array output vector with a single snapshot as mentioned in [28], which leads to the improvement of DOA estimation accuracy. Moreover, as compared with the method in [28], the proposed RVDE method has an extended array aperture that can also help to enhance the estimation accuracy. For convenience, κ_i $(i = 1, 2, \cdots, Q)$ are utilized for the representatives of the Q large eigenvalues of (28), and the DOAs of coherent sources are estimated via

$$\hat{\theta}_{c_k} = \arcsin\left(\frac{\lambda}{\pi d}\arctan(\kappa_k)\right), \quad k = 1, 2, \cdots, Q \tag{29}$$

3.3. Extension to the DOA estimation of the coexistence of the uncorrelated, partially correlated and coherent sources

The proposed RVDE method can be extended to the scenario where the uncorrelated, partially correlated and coherent sources coexist. Due to the incorporation of partially correlated sources, the output vector $\boldsymbol{x}(t)$ defined in (1) can be rewritten as (cf. [15])

$$\boldsymbol{x}(t) = \sum_{k=1}^{P_1}\boldsymbol{a}(\theta_k)s_k(t) + \sum_{k=1}^{P_2}\boldsymbol{a}(\theta_k)s_k(t) + \sum_{k=P+1}^{P+L}\sum_{n=1}^{n_k}\boldsymbol{a}(\theta_{k,n})\varsigma_{k,n}s_k(t) + \boldsymbol{n}(t) \tag{30}$$

where P_1 and P_2 are respectively the number of uncorrelated and partially correlated sources that are collectively referred to as incoherent sources, and $P_1 + P_2 = P$. For this case, both the uncorrelated and partially correlated sources are estimated together in accordance with Section 3.1 firstly. Afterwards, the oblique projection operator defined in (17) is reformulated as $\boldsymbol{C} = \bar{\boldsymbol{A}}_{u,c}(\bar{\boldsymbol{A}}_{u,c}^H\bar{\boldsymbol{R}}^{-1}\bar{\boldsymbol{A}}_{u,c})^{-1}\bar{\boldsymbol{A}}_{u,c}^H\bar{\boldsymbol{R}}^{-1}$ with $\bar{\boldsymbol{A}}_{u,c} = [\boldsymbol{a}(\hat{\theta}_{u_1}), \boldsymbol{a}(\hat{\theta}_{u_2}), \cdots, \boldsymbol{a}(\hat{\theta}_{u_{P_1}}), \boldsymbol{a}(\hat{\theta}_{u_{P_1+1}}), \cdots, \boldsymbol{a}(\hat{\theta}_{u_P})]$ the reconstructed array manifold matrix of the estimated incoherent sources. And then, the remaining coherent sources are resolved by utilizing the methods mentioned in Section 3.2.

The main steps of the proposed RVDE method are summarized as follows.

(1) Construct an augmented matrix $\tilde{\boldsymbol{X}}$, transform it into a real-valued matrix $\hat{\boldsymbol{X}}$, and then calculate the real-valued covariance matrix $\hat{\boldsymbol{R}}$ and the associated real-valued signal subspace $\boldsymbol{E}_s$ according to (2), (4), (5) and (13), respectively.
(2) Evaluate $\boldsymbol{P}_1$, $\boldsymbol{P}_2$ and $\tilde{\boldsymbol{\Omega}}$ according to (8), (9), (14) and (15), and then the DOA estimates of uncorrelated sources $\hat{\theta}_{u_k}$ are obtained via (16). In addition, a selection criterion is utilized to remove the erroneous estimation.
(3) Compute $\hat{\boldsymbol{R}}_c$ according to (17) and (18), construct a real-valued CA-matrix as (22), (26) and (27).
(4) Estimate the DOAs of coherent sources via (29).

4. Discussion

To analyze the proposed RVDE method more comprehensively, the identifiability, computational complexity, the fading coefficient estimation and theoretical MSE of the proposed method are discussed in this section.

4.1. Identifiability

Consider K far-field narrowband sources including P incoherent sources (P_1 uncorrelated sources and P_2 partially correlated sources) and L groups of Q coherent sources impinging on the ULA as described in Section 2. To estimate the uncorrelated sources according to Section 3.1, the inequality $2(M-1) > 2(P+L)$ must be satisfied in light of (14), and hence at least $P+L+1$ sensors are required for the DOA estimation of uncorrelated sources. Moreover, to estimate the coherent sources in accordance with Section 3.2, the dimension of the CA-matrix $\boldsymbol{B}$ defined in (26) determines the minimum number of sensors that can be used for coherent DOA estimation. From this, we know that at least $\lceil 1.25Q - 1\rceil$ sensors are required for the coherent sources. Based on the analysis above, it is clear that the proposed RVDE method requires at least $M = \max\{P + L + 1, \lceil 1.25Q - 1\rceil\}$ sensors to resolve all the incident sources, which implies that more sources than the number of sensors can be resolved with the RVDE method.

Table 1
Comparison of the computational complexity of four methods.

Methods	The number of real-valued multiplications		
	EVD	Moore–Penrose	Spectral search
RVDE	Three times, $22(2M)^2+22(2P+2L)^2+22(M-G+1)^2$	Once, $2(2P+2L)^2(2M-2)+(2P+2L)^3$	Without
EDE	$(M+2)$ times, $4\times 22M^2+22(P+L)^2+4M(22(0.5M+0.5)^2)$	Twice, $4\times(2(P+2L)^2(M-1)+(P+2L)^3)$	Once, $4\times\Delta_s(0.5M+1.5)(0.5M+0.5-Q)$
DEMS	Four times, $4\times 2\times 22M^2+4\times 22(P+L)^2+4\times 22m_s^2$	Once, $4\times(2(P+L)^2(M-1)+(P+L)^3)$	Once, $4\times(\Delta_s(m_s+1)(m_s-K))$
FBSS	Once, $4\times 22m_s^2$	Without	Once, $4\times(\Delta_s(m_s+1)(m_s-K))$

4.2. Computational complexity

To demonstrate the computational efficiency of the proposed RVDE method, the computational complexities of four DOA estimation methods under the coexistence of uncorrelated and coherent sources (the typical complex-valued FBSS method [9], the complex-valued DEMS method [20], the partial real-valued EDE method [22], and the proposed real-valued RVDE method) are discussed in detail. For the reason that a large portion of the computational burden is occupied by the multiplication operations, so the addition operations are negligible. The computational complexity of the proposed real-valued RVDE method mainly includes:

(1) The real-valued EVD (based on the QZ step [33]) of $\hat{\boldsymbol{R}}$ costs about $22(2M)^2$ real-valued multiplications.
(2) The real-valued Moore–Penrose operation of $(\boldsymbol{P}_1\boldsymbol{E}_s)^{\dagger}$ needs about $2(2P+2L)^2(2M-2)+(2P+2L)^3$ real-valued multiplications.
(3) The real-valued EVD of $\tilde{\boldsymbol{\Omega}}$ requires about $22(2P+2L)^2$ real-valued multiplications.
(4) The real-valued EVD of (28) requires about $22(M-G+1)^2$ real-valued multiplications.

Table 1 presents the comparison of computational complexity of the four methods in terms of the number of real-valued multiplications (one complex-valued multiplication is equivalent to four real-valued multiplications), in which the main computational load originated from the operations of EVD, Moore–Penrose and spectral search are considered. In Table 1, m_s denotes the number of sensors in a subarray and Δ_s denotes the number of the total sample points of the MUSIC spatial spectrum over $[-\pi/2,\pi/2]$.

According to Table 1, the total computational complexities of the RVDE, EDE, FBSS and DEMS methods are approximately given by

$$C_{RVDE}=110M^2+16P^2M+16L^2M+32PLM-44GM \tag{31}$$

$$C_{EDE}=22M^3+132M^2+8P^2M+32L^2M+32PLM+\Delta_s(M^2-2MQ) \tag{32}$$

$$C_{FBSS}=88m_s^2+4\Delta_s(m_s^2-m_sK) \tag{33}$$

$$C_{DEMS}=176M^2+88m_s^2+8P^2M+8L^2M+16PLM+4\Delta_s(m_s^2-m_sK) \tag{34}$$

Compared with (31) and (32), it is clear that $C_{EDE}=C_{RVDE}+22M^3+22M^2+16L^2M-8P^2M+44GM+\Delta_s(M^2-2MQ)$ holds, wherein $\Delta_s\gg M$ owing to the intensive spectral search involved in the EDE method. This implies that the EDE method requires more computational burdens than the RVDE method. Note that it is hard to compare the computational complexity of RVDE with that of FBSS via (31) and (33) intuitively. Thus, a numerical example is taken for the comparison of (31) and (33), where several typical values are given under conditions that $M/3\le G\le M/2$ and $K+1\le m_s\le M-K+1$. For spectral search with step 0.5°, Δ_s is equivalent to 360. The other related typical values are set to be $M=8$, $m_s=5$, $G=3$, $P=2$, $Q=2$, $L=1$. In this case, the RVDE and the FBSS methods require 7136 and 9400 real-valued multiplications respectively according to (31) and (33), which indicates that the computational burden of the RVDE method has decreased by more than 31% as compared to the FBSS method. When Δ_s increases in the case of finer spectral search, the computational complexity of the FBSS method C_{FBSS} also increases. Furthermore, it is easily known from (33) and (34) that the DEMS method is more computationally expensive than that of the FBSS method (i.e., $C_{DEMS}=C_{FBSS}+88M^2+8P^2M+8L^2M+16PLM$), although both of them require spectral search operations. In summary, the proposed RVDE method has much lower computational complexity as compared to the FBSS, the DEMS and EDE methods.

4.3. The estimation of fading coefficients

To illustrate the property of multipath propagation clearly, the knowledge of fading coefficients requires to be estimated. Since the DOAs of coherent sources have been estimated by (29), the reconstructed array manifold matrix of coherent sources is established as $\bar{\boldsymbol{A}}_{c,k}=[\boldsymbol{a}(\hat{\theta}_{c_{k,1}}),\boldsymbol{a}(\hat{\theta}_{c_{k,2}}),\cdots,\boldsymbol{a}(\hat{\theta}_{c_{k,n_k}})]$, $k=P+1,P+2,\cdots,P+L$. Then the fading coefficient estimation can be determined by a modified constraint quadratic minimization problem

$$\hat{\boldsymbol{\varsigma}}_k=\arg\min_{\boldsymbol{\varsigma}_k}\left\|\boldsymbol{V}_n^H\bar{\boldsymbol{A}}_{c,k}\boldsymbol{\varsigma}_k\right\|^2+\beta\|\boldsymbol{\varsigma}_k\|^2\quad s.t.\quad \boldsymbol{\varsigma}_k^H\boldsymbol{w}_k\equiv 1 \tag{35}$$

where $\beta>0$ is a penalty factor that is set to $\beta=0.01$ in the simulations, and $\boldsymbol{w}_k=[1,0,\cdots,0]^T$ is a $1\times n_k$ row vector for $k=1,2,\cdots,L$. The solution can be obtained by exploiting the method of Lagrange multipliers [31] as

$$\hat{\boldsymbol{\varsigma}}_k=\frac{(\bar{\boldsymbol{A}}_{c,k}^H\boldsymbol{V}_n\boldsymbol{V}_n^H\bar{\boldsymbol{A}}_{c,k}+\beta\boldsymbol{I}_{n_k})^{-1}\boldsymbol{w}_k}{\boldsymbol{w}_k^H(\bar{\boldsymbol{A}}_{c,k}^H\boldsymbol{V}_n\boldsymbol{V}_n^H\bar{\boldsymbol{A}}_{c,k}+\beta\boldsymbol{I}_{n_k})^{-1}\boldsymbol{w}_k} \tag{36}$$

The modified fading coefficient estimation (MFCE) criterion is different from the method in [31], because the fading coefficient estimation problem is transformed into a modified constraint quadratic minimization problem by adding penalties, which guarantees the stability of the solution.

4.4. The theoretical MSE

In order to illustrate the favorable performance of the proposed RVDE method, the theoretical MSEs of DOA estimates for uncorrelated and coherent sources are given as follows (see Appendix C for details)

$$\mathrm{var}(\theta_{u_k}) = \frac{\pi^2}{-\frac{4}{9}\eta_k^4 + \frac{8}{3}\eta_k^2 - 4 + \pi^2\eta_k^{-2}} \times \left(\frac{1}{N} \left(\boldsymbol{e}_k^T (\boldsymbol{P}_1 \hat{\boldsymbol{A}})^\dagger (\Delta\boldsymbol{A}_2 - \Delta\boldsymbol{A}_1)(\Delta\boldsymbol{A}_2 - \Delta\boldsymbol{A}_1)^T \times \left(\boldsymbol{e}_k^T (\boldsymbol{P}_1 \hat{\boldsymbol{A}})^\dagger \right)^T \right) \right) \tag{37}$$

$$\mathrm{var}(\theta_{c_k}) = \frac{\pi^2}{-\frac{4}{9}\kappa_k^4 + \frac{8}{3}\kappa_k^2 - 4 + \pi^2\kappa_k^{-2}} \times \left(\frac{1}{N} \left(\boldsymbol{e}_k^T \left(\mathrm{Re}\{ \boldsymbol{Q}_{M-G}^H \boldsymbol{K}_1^{M-G} \boldsymbol{Q}_{M-G+1} \} \right)^\dagger \times (\Delta\boldsymbol{K}_2 - \Delta\boldsymbol{K}_1)(\Delta\boldsymbol{K}_2 - \Delta\boldsymbol{K}_1)^T \times \left(\boldsymbol{e}_k^T \left(\mathrm{Re}\{ \boldsymbol{Q}_{M-G}^H \boldsymbol{K}_1^{M-G} \boldsymbol{Q}_{M-G+1} \} \right)^\dagger \right)^T \right) \right) \tag{38}$$

where $\boldsymbol{e}_k$ is a unit vector with one at the kth element and zero elsewhere. $\Delta\boldsymbol{A}_1$, $\Delta\boldsymbol{A}_2$, $\Delta\boldsymbol{K}_1$ and $\Delta\boldsymbol{K}_2$ represent the disturbance error of $\boldsymbol{P}_1\hat{\boldsymbol{A}}$, $\boldsymbol{P}_2\hat{\boldsymbol{A}}$, $\mathrm{Re}\{\boldsymbol{Q}_{M-G}^H \boldsymbol{K}_1^{M-G} \boldsymbol{Q}_{M-G+1}\}$ and $\mathrm{Im}\{\boldsymbol{Q}_{M-G}^H \boldsymbol{K}_1^{M-G} \boldsymbol{Q}_{M-G+1}\}$, respectively, which satisfy that $\Delta\boldsymbol{A}_1 \propto \frac{1}{SNR}$, $\Delta\boldsymbol{A}_2 \propto \frac{1}{SNR}$, $\Delta\boldsymbol{K}_1 \propto \frac{1}{SNR}$ and $\Delta\boldsymbol{K}_2 \propto \frac{1}{SNR}$. Note that the theoretical MSEs of uncorrelated source and the coherent sources mainly depend on the disturbance error and they tend to increase with the increase of disturbance error. More specially, the disturbance errors tend to be zero (i.e., $\Delta\boldsymbol{A}_1 \to 0$, $\Delta\boldsymbol{A}_2 \to 0$, $\Delta\boldsymbol{K}_1 \to 0$ and $\Delta\boldsymbol{K}_2 \to 0$) in ideal cases, we have $\mathrm{var}(\theta_{u_k}) \to 0$ and $\mathrm{var}(\theta_{c_k}) \to 0$ accordingly.

5. Simulation results

In this section, we consider a mixture of uncorrelated and coherent sources impinging on an 8-sensor ULA with interspacing $\lambda/2$ in the following simulations, and all the simulation results are averaged over 2000 independent Monte Carlo trials.

5.1. DOA estimation

Several simulations are presented to illustrate the DOA estimation performance of the proposed RVDE method wherein the existing partial real-valued EDE method [22], the complex-valued DEMS method [20], and the traditional complex-valued FBSS method [9] are selected as comparative methods as well as the theoretical average root mean square error (RMSE) and the Cramér–Rao bound (CRB). The RMSE is referred to as a significant performance index for evaluating the performance of DOA estimation, which is defined as

$$RMSE = \sqrt{\frac{1}{2000K} \sum_{i=1}^{2000} \left(\sum_{k=1}^{P} (\hat{\theta}_{u_{k,i}} - \theta_{u_k})^2 + \sum_{k=1}^{Q} (\hat{\theta}_{c_{k,i}} - \theta_{c_k})^2 \right)} \tag{39}$$

where $\hat{\theta}_{u_{k,i}}$ and $\hat{\theta}_{c_{k,i}}$ are the estimates of θ_{u_k} and θ_{c_k} in the ith Monte Carlo trial respectively, and K denotes the total number of all incident sources that satisfies $K = P + Q$. With (37) and (38), the theoretical RMSE of a mixture of uncorrelated and coherent sources are obtained from

$$RMSE_{theory} = \sqrt{\frac{1}{K} \left(\sum_{k=1}^{P} \mathrm{var}(\theta_{u_k}) + \sum_{k=1}^{Q} \mathrm{var}(\theta_{c_k}) \right)} \tag{40}$$

In the first simulation, we compare the DOA estimation results of the RVDE, EDE, DEMS and FBSS methods intuitively. Assuming that two uncorrelated sources come from [25.8° 43.4°] and one group of three coherent sources comes from [−21.3° −13.5° 30.2°] with the fading coefficients $[1, -0.5280 + 0.6010j, 0.9335 - 0.3585j]$. The SNR and the number of snapshots are set to be 10 dB and 500, respectively. For the EDE, DEMS and FBSS methods that involve spectral search, the search step is set to be 0.5°. Fig. 1 presents the DOA estimation results of the four methods. It can be seen from Fig. 1 that although all of the four methods are able to estimate DOAs of the uncorrelated and coherent sources, the proposed RVDE method yields the minimum estimate errors relative to the incident angles.

To demonstrate the computational efficiency of the proposed method, we evaluate the averaged CPU times (in MATLAB 7.8 (R2009a) on a 2.8 GHz 4 GB PC) of the four methods versus the number of snapshots over 2000 independent Monte Carlo trials, and the results are presented in Table 2. It can be observed from Table 2 that the proposed RVDE method costs the shortest computation time, which is mainly attributed to the following reasons. The RVDE method is implemented in the real-valued domain and it requires no spectral search. By contrast, the DEMS and FBSS methods are performed with complex-valued computations and the EDE method operates with partial real-valued computations and partial complex-valued computations. Besides, the computationally expensive spectral search is inevitable in these methods.

In the second simulation, we compare the estimation performance of the RVDE method with that of the comparative methods versus SNR and the number of snapshots. The incident source mode is the same as that in the first simulation, and the results are shown in Fig. 2 and Fig. 3, respectively. It can be concluded from Fig. 2 and Fig. 3 that the proposed RVDE method outperforms the EDE, DEMS and FBSS methods in terms of RMSE, especially for the scenarios of low SNR or small number of snapshots. This is due to the fact that the proposed RVDE method is performed by constructing the augmented matrices, which enlarges the effective array aperture, and the DOA estimation accuracy is improved accordingly. It should also be noted that the oblique projection technique is exploited to eliminate the uncorrelated sources in the RVDE method, which causes no power lost of coherent sources. By contrast, the power lost occurs in the EDE and the DEMS methods due to the differencing processing. Moreover, the proposed RVDE method estimates both the uncorrelated and the coherent sources in the real-valued domain, which significantly reduces the computational burden, while the EDE method estimates the DOAs of coherent source in the complex-valued domain and the DEMS and the FBSS methods estimate all the incident sources in the complex-valued domain.

The third simulation considers the scenario that the number of incident sources goes beyond that of sensors. Consider that five uncorrelated sources [−18.4° −10.9° 27.8° 38.1° 45.2°] and two groups of coherent sources are coming from [−24.9° 22.2°] and [−47.1° 13.5°] with fading coefficients $[1, -0.0153 + 0.8999j]$ and $[1, 0.4956 + 0.4944j]$. Fig. 4 plots the RMSE versus SNR with the fixed number of snapshots 1000, and the RMSE versus number of snapshots is depicted in Fig. 5 with the fixed SNR 15 dB. Note that the minimum number of sensors that required by the methods outlined in [22] and [9] are 9 and 14 respectively under the premise that all the incident sources must be detected. Therefore, both the EDE method and FBSS method fail to resolve all the sources in this simulation when an 8-sensor ULA is employed.

As can be seen from Fig. 4 and Fig. 5 that both the RVDE and the DEMS methods can detect all the 9 DOAs of incident sources correctly, which implies that the two methods can resolve more sources than the number of sensors. However, the RVDE method can provide more accurate DOA estimates than the DEMS method.

The fourth simulation compares the resolving ability of the four methods by investigating the effect of angular separation between uncorrelated and coherent sources on the DOA estimation

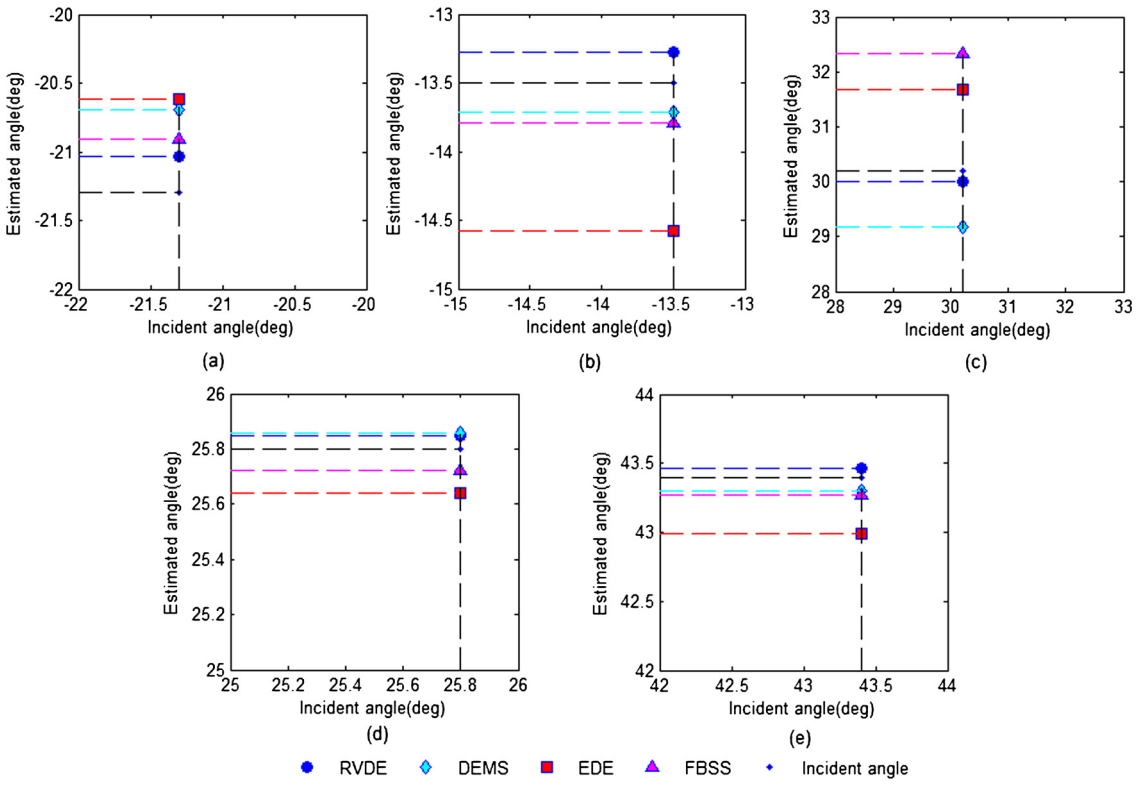

Fig. 1. DOA estimation with the fixed SNR 10 dB and number of snapshots 500 (a) the first coherent source (b) the second coherent source (c) the third coherent source (d) the first uncorrelated source (e) the second uncorrelated source.

Table 2
Averaged CPU times.

Number of snapshots	Time (sec)			
	RVDE	EDE	DEMS	FBSS
100	0.0024	0.0080	0.0049	0.0040
300	0.0052	0.0119	0.0094	0.0066
500	0.0096	0.0168	0.0131	0.0117

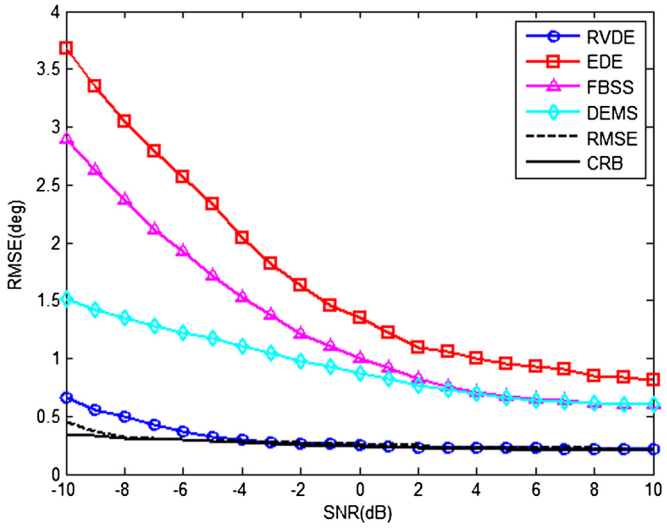

Fig. 2. RMSE versus SNR with the fixed number of snapshots 500.

performance. In this simulation, one uncorrelated source comes from 16.5° and a group of two coherent sources comes from $[-22.1°\ 16.5° + \Delta\theta]$, where $\Delta\theta$ is varied from 0° to 10° with a step size of 1°. The fading coefficients are $[1, -0.3358 - 0.7261j]$.

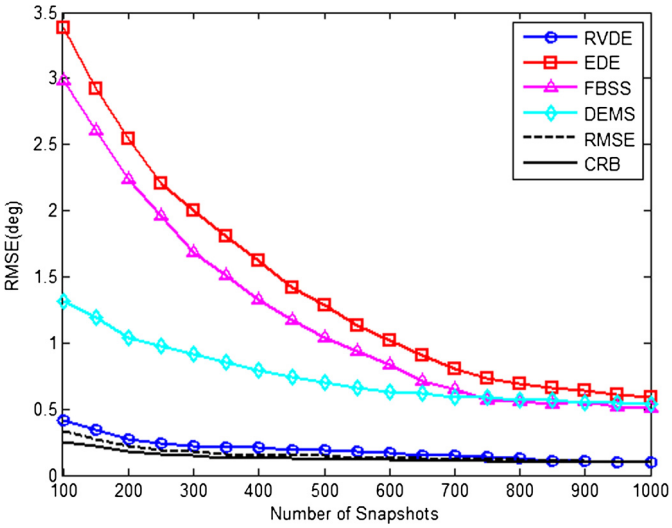

Fig. 3. RMSE versus number of snapshots with the fixed SNR 2 dB.

Fig. 6 depicts the bias (the difference between the estimated angle and the true angle) versus angular separation with the fixed SNR 5 dB and number of snapshots 300.

Fig. 6 shows that the RVDE method provides a smaller bias as compared to the EDE, DEMS and FBSS methods for both uncorrelated and coherent sources, and the bias becomes smaller with the increase of angular separation. It is also seen from Fig. 6 that the FBSS method fails to work when the angular separation is less than 4°. The reason is that the RVDE, DEMS and EDE methods estimate the DOAs of uncorrelated and coherent sources separately, thus these methods can resolve the uncorrelated and coherent sources correctly even the angular separation is 0°. By contrast,

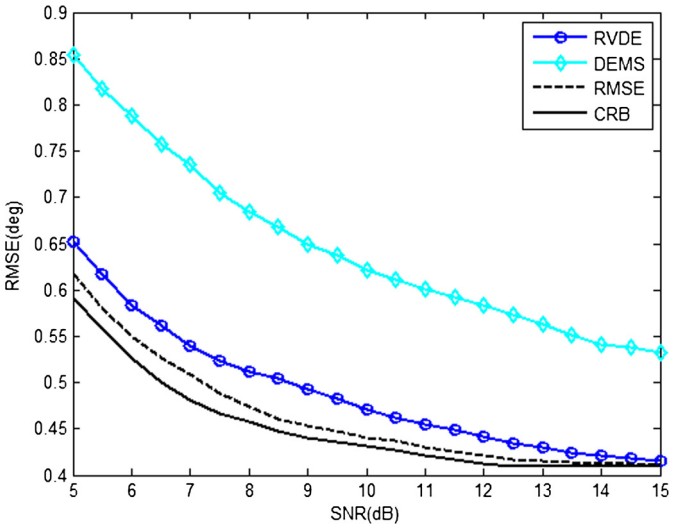

Fig. 4. RMSE versus SNR with the fixed number of snapshots 1000.

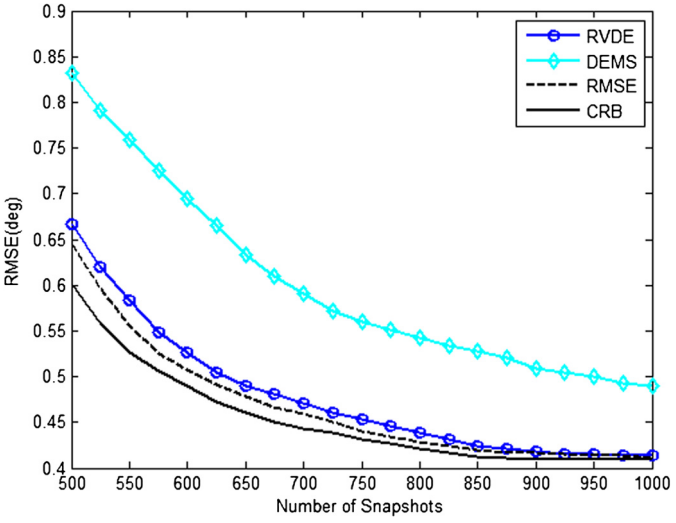

Fig. 5. RMSE versus number of snapshots with the fixed SNR 15 dB.

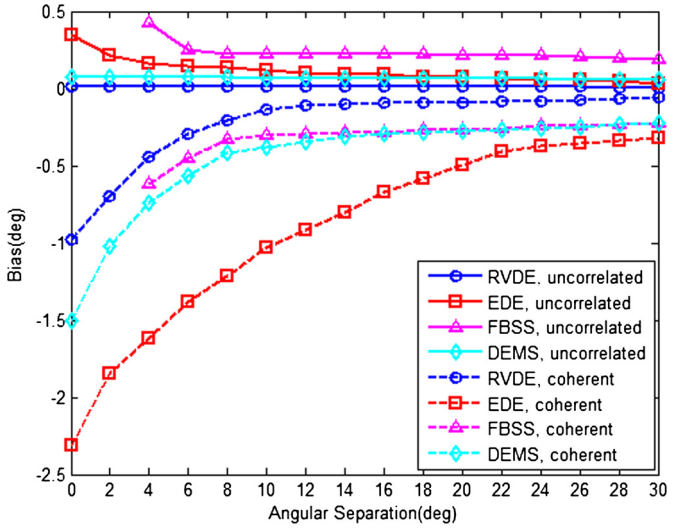

Fig. 6. Bias versus angular separation with the fixed SNR 5 dB and number of snapshots 300.

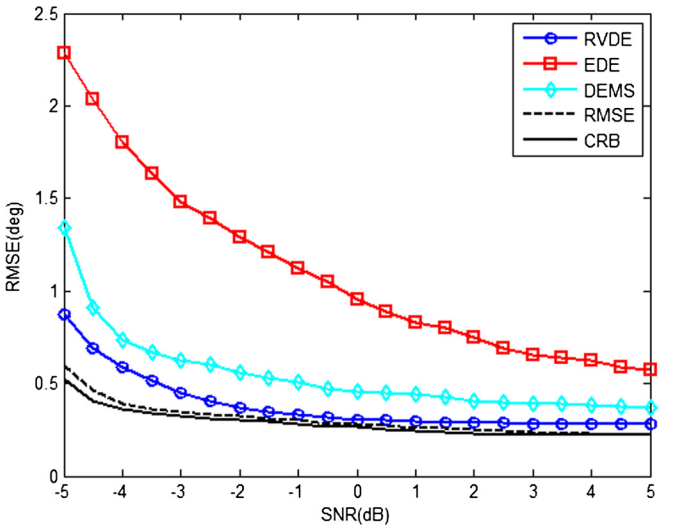

Fig. 7. RMSE versus SNR with the fixed number of snapshots 1000 and $\rho e^{j\alpha} = 0.3e^{j117.93^\circ}$.

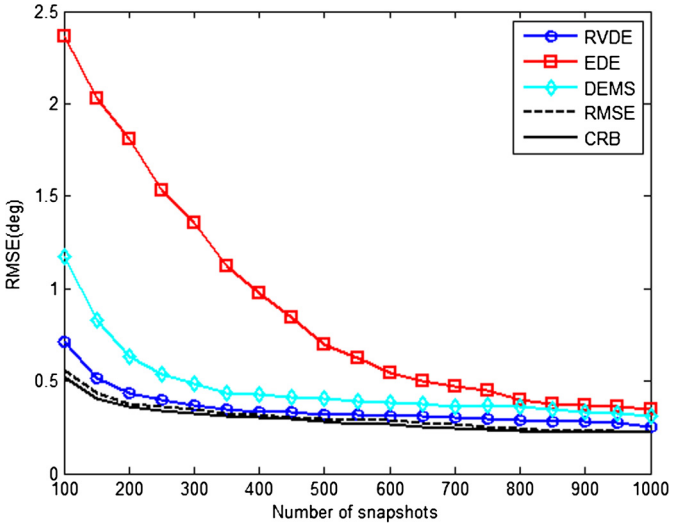

Fig. 8. RMSE versus number of snapshots with the fixed SNR 5 dB and $\rho e^{j\alpha} = 0.3e^{j117.93^\circ}$.

the FBSS method estimates the uncorrelated and coherent source simultaneously, so that it would suffer from serious degradation in case of small angular separation.

In the fifth simulation, we extend the RVDE method to the scenario where the uncorrelated, partially correlated and coherent sources coexist. There are two uncorrelated sources [14.7° 33.1°], two partially correlated sources [22.2° 70.1°] correlation and one group of coherent sources [−30.4° 7.2°]. The fading coefficients of the coherent sources are $[1, 0.4469 - 0.7696j]$, and the correlation coefficient between two partially correlated sources can be denoted as $\rho e^{j\alpha}$. The RMSE versus SNR and number of snapshots with different correlation coefficients are shown in Fig. 7, Fig. 8, Fig. 9 and Fig. 10. It is known from [16] that FBSS method will fail in such scenario.

The results from Fig. 7 to Fig. 10 illustrate that the RVDE method can be extended to the scenario where the uncorrelated, partially correlated and coherent sources coexist. Also, the proposed RVDE method has a better performance than the EDE and DEMS methods, which follows the same reason as that in the second simulation.

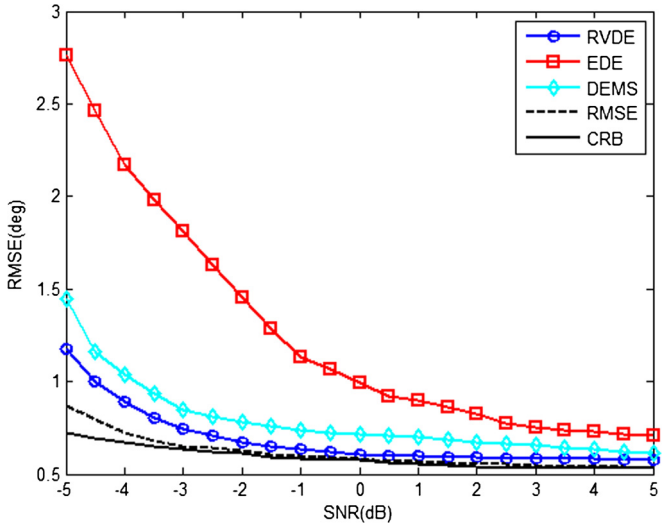

Fig. 9. RMSE versus SNR with the fixed number of snapshots 1000 and $\rho e^{j\alpha} = 0.7e^{j65.34^\circ}$.

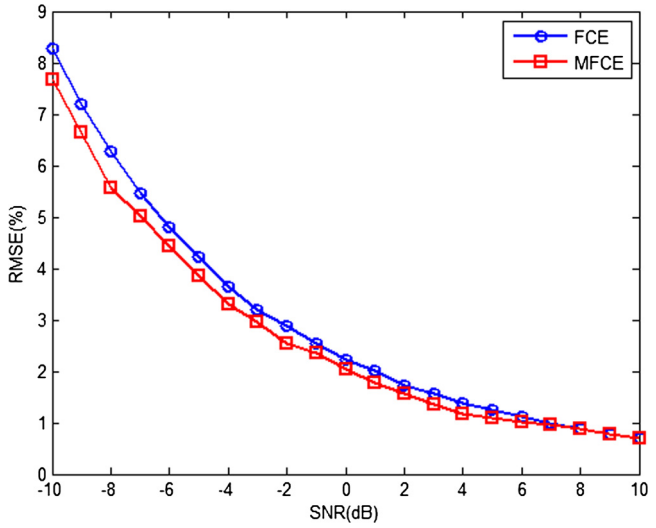

Fig. 11. RMSE of fading coefficient estimations versus SNR with the fixed number of snapshots 300.

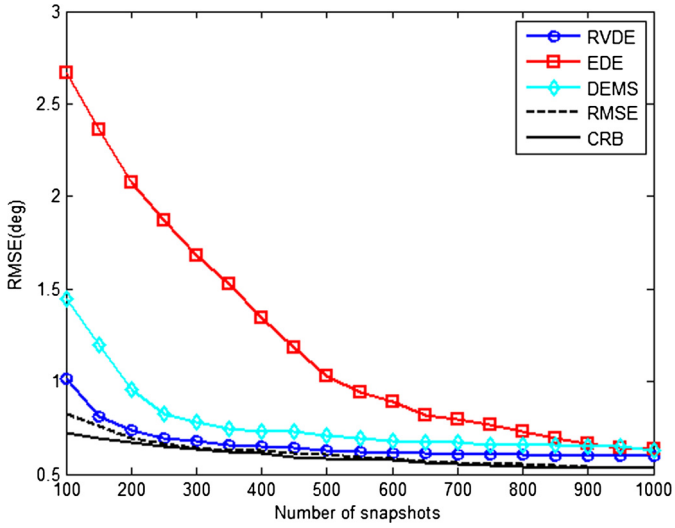

Fig. 10. RMSE versus number of snapshots with the fixed SNR 5 dB and $\rho e^{j\alpha} = 0.7e^{j65.34^\circ}$.

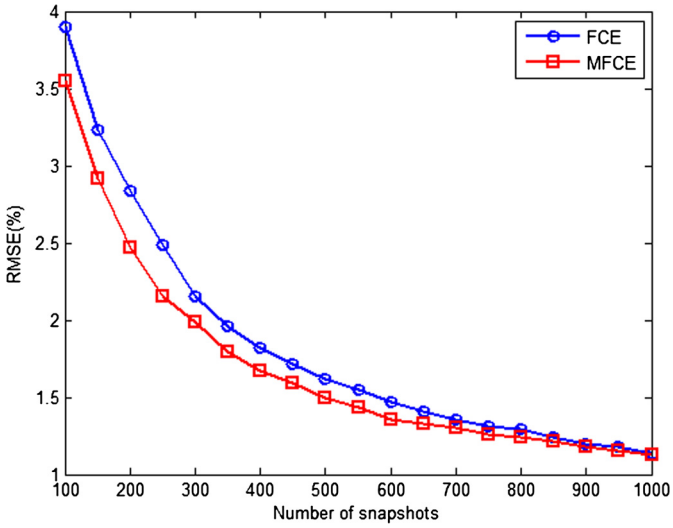

Fig. 12. RMSE of fading coefficient estimations versus number of snapshots with the fixed SNR 0 dB.

5.2. Fading coefficient estimation

This simulation studies fading coefficient estimation of coherent sources. The fading coefficients estimation (FEC) [31] is chosen for comparison. All the conditions are the same as the fourth simulation in Section 5.1, except that $\Delta\theta$ is fixed at $\Delta\theta = 10^\circ$ in this simulation. On the basis of the RVDE method, the DOA estimates of coherent sources are utilized as the prior for the fading coefficient estimation. The RMSE of fading coefficient estimation is defined as

$$RMSE_{\boldsymbol{\Upsilon}} = \sqrt{\frac{1}{2000\|\boldsymbol{\Upsilon}\|^2}\sum_{i=1}^{2000}\|\hat{\boldsymbol{\Upsilon}}_i - \boldsymbol{\Upsilon}\|^2} \times 100\% \tag{41}$$

where $\hat{\boldsymbol{\Upsilon}}_i$ represents the estimate of $\boldsymbol{\Upsilon}$ in the ith Monte Carlo trial. The RMSEs of the fading coefficient estimations versus SNR and number of snapshots are shown in Fig. 11 and Fig. 12, respectively. It is indicated in Fig. 11 and Fig. 12 that the proposed MFCE criterion outperforms the FEC criterion in the unfavorable cases (low SNR or the snapshot number), while for the favorable cases (large SNR or the snapshot number) the two criterions have the similar performance. This is because the MFCE criterion is developed by incorporating the penalty factor into a constraint quadratic minimization problem, which guarantees the stability of the solution, especially for the unfavorable cases. By contrast, in the favorable cases, the contribution of the penalty factor tends to be less distinct, and the performance of the two criterions tends to be consistent.

6. Conclusion

In this paper, a novel RVDE method is proposed for a mixture of uncorrelated and coherent sources. The proposed method firstly estimates the DOAs of uncorrelated sources by employing a real-valued augmented matrix. Then, in order to remove the contributions of the uncorrelated sources, an oblique projection operator is adopted. Afterwards, a real-valued coherent augmented matrix is constructed for coherent DOA estimation. By applying the unitary transformation, the RVDE method achieves DOA estimation of both the uncorrelated and coherent sources in the real-valued domain, which significantly reduces the computational complexity. With the estimated DOAs of coherent sources, the fading coefficients are estimated by adding penalties to a constraint quadratic minimization problem, which guarantees the stability of the so-

lution. Simulation results show that the RVDE method can detect more sources than the number of sensors and has more notable performance advantages than the EDE, DEMS and FBSS methods in estimation accuracy and computational burden. Moreover, the RVDE method can be extended to the scenario that the uncorrelated, partially correlated and coherent sources coexist.

Acknowledgments

This work was supported by Aviation Science Foundation of China (201401P6001) and Fundamental Research Funds for the Central Universities (HEUCF150804)

Appendix A

In this appendix, we prove that (12) holds. Based on (11), we have

$$\begin{aligned}\boldsymbol{\Omega} &= (\boldsymbol{P}_1\hat{\boldsymbol{A}})^{\dagger}\boldsymbol{P}_2\hat{\boldsymbol{A}}\\ &= \left(\boldsymbol{Q}_{2M-2}^{H}(\boldsymbol{I}_2\otimes(\boldsymbol{K}_1^{M-1}+\boldsymbol{K}_2^{M-1}))\boldsymbol{Q}_{2M}\boldsymbol{Q}_{2M}^{H}(\boldsymbol{I}_2\otimes\boldsymbol{A})\right)^{\dagger}\\ &\quad\times\left(\boldsymbol{Q}_{2M-2}^{H}j(\boldsymbol{I}_2\otimes(\boldsymbol{K}_1^{M-1}-\boldsymbol{K}_2^{M-1}))\right.\\ &\quad\left.\times\,\boldsymbol{Q}_{2M}\boldsymbol{Q}_{2M}^{H}(\boldsymbol{I}_2\otimes\boldsymbol{A})\right)\end{aligned}\tag{A.1}$$

For notational convenience, $\boldsymbol{K}_1$ and $\boldsymbol{K}_2$ are regarded as the abbreviated forms of $\boldsymbol{K}_1^{M-1}$ and $\boldsymbol{K}_2^{M-1}$, respectively.

Note that $\boldsymbol{Q}_m\boldsymbol{Q}_m^{H}=\boldsymbol{I}_m$, and (A.1) can be further expressed as

$$\begin{aligned}\boldsymbol{\Omega} &= \left((\boldsymbol{I}_2^{H}\otimes(\boldsymbol{A}^{H}\boldsymbol{K}_1^{H}+\boldsymbol{A}^{H}\boldsymbol{K}_2^{H}))\times(\boldsymbol{I}_2\otimes(\boldsymbol{K}_1\boldsymbol{A}+\boldsymbol{K}_2\boldsymbol{A}))\right)^{-1}\\ &\quad\times\left((\boldsymbol{I}_2^{H}\otimes(\boldsymbol{A}^{H}\boldsymbol{K}_1^{H}+\boldsymbol{A}^{H}\boldsymbol{K}_2^{H}))\times j(\boldsymbol{I}_2\otimes(\boldsymbol{K}_1\boldsymbol{A}-\boldsymbol{K}_2\boldsymbol{A}))\right)\\ &= j\left(\boldsymbol{I}_2^{H}\boldsymbol{I}_2\otimes([\boldsymbol{A}_u,\boldsymbol{A}_c\boldsymbol{\Upsilon}]^{H}(\boldsymbol{K}_1^{H}+\boldsymbol{K}_2^{H})(\boldsymbol{K}_1+\boldsymbol{K}_2)[\boldsymbol{A}_u,\boldsymbol{A}_c\boldsymbol{\Upsilon}])\right)^{-1}\\ &\quad\times\left(\boldsymbol{I}_2^{H}\boldsymbol{I}_2\otimes([\boldsymbol{A}_u,\boldsymbol{A}_c\boldsymbol{\Upsilon}]^{H}(\boldsymbol{K}_1^{H}+\boldsymbol{K}_2^{H})(\boldsymbol{K}_1-\boldsymbol{K}_2)[\boldsymbol{A}_u,\boldsymbol{A}_c\boldsymbol{\Upsilon}])\right)\\ &= j\left(\boldsymbol{I}_2\otimes\left(([\boldsymbol{A}_{u_1},\boldsymbol{A}_{c_1}\boldsymbol{\Upsilon}]+[\boldsymbol{A}_{u_2},\boldsymbol{A}_{c_2}\boldsymbol{\Upsilon}])^{H}\right.\right.\\ &\quad\times\left.\left.([\boldsymbol{A}_{u_1},\boldsymbol{A}_{c_1}\boldsymbol{\Upsilon}]+[\boldsymbol{A}_{u_2},\boldsymbol{A}_{c_2}\boldsymbol{\Upsilon}]))\right)^{-1}\right.\\ &\quad\times\left(\boldsymbol{I}_2\otimes\left(([\boldsymbol{A}_{u_1},\boldsymbol{A}_{c_1}\boldsymbol{\Upsilon}]+[\boldsymbol{A}_{u_2},\boldsymbol{A}_{c_2}\boldsymbol{\Upsilon}])^{H}\right.\right.\\ &\quad\left.\left.\times([\boldsymbol{A}_{u_1},\boldsymbol{A}_{c_1}\boldsymbol{\Upsilon}]-[\boldsymbol{A}_{u_2},\boldsymbol{A}_{c_2}\boldsymbol{\Upsilon}]))\right)\right)\end{aligned}\tag{A.2}$$

It is easy to see that $\boldsymbol{A}_{u_2}=\boldsymbol{A}_{u_1}\boldsymbol{\Delta}_u$ and $\boldsymbol{A}_{c_2}=\boldsymbol{A}_{c_1}\boldsymbol{\Delta}_c$, and (A.2) can be rewritten as

$$\begin{aligned}\boldsymbol{\Omega} &= j\left(\boldsymbol{I}_2\otimes\left(([\boldsymbol{A}_{u_1},\boldsymbol{A}_{c_1}\boldsymbol{\Upsilon}]+[\boldsymbol{A}_{u_1}\boldsymbol{\Delta}_u,\boldsymbol{A}_{c_1}\boldsymbol{\Delta}_c\boldsymbol{\Upsilon}])^{H}\right.\right.\\ &\quad\times\left.\left.([\boldsymbol{A}_{u_1},\boldsymbol{A}_{c_1}\boldsymbol{\Upsilon}]+[\boldsymbol{A}_{u_1}\boldsymbol{\Delta}_u,\boldsymbol{A}_{c_1}\boldsymbol{\Delta}_c\boldsymbol{\Upsilon}]))\right)^{-1}\right.\\ &\quad\times\left(\boldsymbol{I}_2\otimes\left(([\boldsymbol{A}_{u_1},\boldsymbol{A}_{c_1}\boldsymbol{\Upsilon}]+[\boldsymbol{A}_{u_1}\boldsymbol{\Delta}_u,\boldsymbol{A}_{c_1}\boldsymbol{\Delta}_c\boldsymbol{\Upsilon}])^{H}\right.\right.\\ &\quad\left.\left.\times([\boldsymbol{A}_{u_1},\boldsymbol{A}_{c_1}\boldsymbol{\Upsilon}]-[\boldsymbol{A}_{u_1}\boldsymbol{\Delta}_u,\boldsymbol{A}_{c_1}\boldsymbol{\Delta}_c\boldsymbol{\Upsilon}]))\right)\right)\end{aligned}\tag{A.3}$$

Denote $\boldsymbol{\Theta}_{u+}=\boldsymbol{I}_P+\boldsymbol{\Delta}_u$, $\boldsymbol{\Theta}_{u-}=\boldsymbol{I}_P-\boldsymbol{\Delta}_u$, $\boldsymbol{\Theta}_{c+}=\boldsymbol{I}_Q+\boldsymbol{\Delta}_c$ and $\boldsymbol{\Theta}_{c-}=\boldsymbol{I}_Q-\boldsymbol{\Delta}_c$, thus $\boldsymbol{\Omega}$ can be simplified to

$$\begin{aligned}\boldsymbol{\Omega} &= j\left(\boldsymbol{I}_2\otimes([\boldsymbol{A}_{u_1}\boldsymbol{\Theta}_{u+},\boldsymbol{A}_{c_1}\boldsymbol{\Theta}_{c+}\boldsymbol{\Upsilon}]^{H}\times[\boldsymbol{A}_{u_1}\boldsymbol{\Theta}_{u+},\boldsymbol{A}_{c_1}\boldsymbol{\Theta}_{c+}\boldsymbol{\Upsilon}])\right)^{-1}\\ &\quad\times\left(\boldsymbol{I}_2\otimes([\boldsymbol{A}_{u_1}\boldsymbol{\Theta}_{u+},\boldsymbol{A}_{c_1}\boldsymbol{\Theta}_{c+}\boldsymbol{\Upsilon}]^{H}\times[\boldsymbol{A}_{u_1}\boldsymbol{\Theta}_{u-},\boldsymbol{A}_{c_1}\boldsymbol{\Theta}_{c-}\boldsymbol{\Upsilon}])\right)\\ &= j\left(\boldsymbol{I}_2^{-1}\otimes\begin{bmatrix}\boldsymbol{\Theta}_{u+}^{H}\boldsymbol{A}_{u1}^{H}\boldsymbol{A}_{u_1}\boldsymbol{\Theta}_{u+} & \boldsymbol{\Theta}_{u+}^{H}\boldsymbol{A}_{u1}^{H}\boldsymbol{A}_{c_1}\boldsymbol{\Theta}_{c+}\boldsymbol{\Upsilon}\\ \boldsymbol{\Upsilon}^{H}\boldsymbol{\Theta}_{c+}^{H}\boldsymbol{A}_{c1}^{H}\boldsymbol{A}_{u_1}\boldsymbol{\Theta}_{u+} & \boldsymbol{\Upsilon}^{H}\boldsymbol{\Theta}_{c+}^{H}\boldsymbol{A}_{c1}^{H}\boldsymbol{A}_{c_1}\boldsymbol{\Theta}_{c+}\boldsymbol{\Upsilon}\end{bmatrix}^{-1}\right)\\ &\quad\times\left(\boldsymbol{I}_2\otimes\begin{bmatrix}\boldsymbol{\Theta}_{u+}^{H}\boldsymbol{A}_{u1}^{H}\boldsymbol{A}_{u_1}\boldsymbol{\Theta}_{u-} & \boldsymbol{\Theta}_{u+}^{H}\boldsymbol{A}_{u1}^{H}\boldsymbol{A}_{c_1}\boldsymbol{\Theta}_{c-}\boldsymbol{\Upsilon}\\ \boldsymbol{\Upsilon}^{H}\boldsymbol{\Theta}_{c+}^{H}\boldsymbol{A}_{c1}^{H}\boldsymbol{A}_{u_1}\boldsymbol{\Theta}_{u-} & \boldsymbol{\Upsilon}^{H}\boldsymbol{\Theta}_{c+}^{H}\boldsymbol{A}_{c1}^{H}\boldsymbol{A}_{c_1}\boldsymbol{\Theta}_{c-}\boldsymbol{\Upsilon}\end{bmatrix}\right)\\ &= j\boldsymbol{I}_2\otimes\left(\begin{bmatrix}\boldsymbol{\Theta}_{u+}^{H}\boldsymbol{A}_{u1}^{H}\boldsymbol{A}_{u_1}\boldsymbol{\Theta}_{u+} & \boldsymbol{\Theta}_{u+}^{H}\boldsymbol{A}_{u1}^{H}\boldsymbol{A}_{c_1}\boldsymbol{\Theta}_{c+}\boldsymbol{\Upsilon}\\ \boldsymbol{\Upsilon}^{H}\boldsymbol{\Theta}_{c+}^{H}\boldsymbol{A}_{c1}^{H}\boldsymbol{A}_{u_1}\boldsymbol{\Theta}_{u+} & \boldsymbol{\Upsilon}^{H}\boldsymbol{\Theta}_{c+}^{H}\boldsymbol{A}_{c1}^{H}\boldsymbol{A}_{c_1}\boldsymbol{\Theta}_{c+}\boldsymbol{\Upsilon}\end{bmatrix}^{-1}\right.\\ &\quad\left.\times\begin{bmatrix}\boldsymbol{\Theta}_{u+}^{H}\boldsymbol{A}_{u1}^{H}\boldsymbol{A}_{u_1}\boldsymbol{\Theta}_{u-} & \boldsymbol{\Theta}_{u+}^{H}\boldsymbol{A}_{u1}^{H}\boldsymbol{A}_{c_1}\boldsymbol{\Theta}_{c-}\boldsymbol{\Upsilon}\\ \boldsymbol{\Upsilon}^{H}\boldsymbol{\Theta}_{c+}^{H}\boldsymbol{A}_{c1}^{H}\boldsymbol{A}_{u_1}\boldsymbol{\Theta}_{u-} & \boldsymbol{\Upsilon}^{H}\boldsymbol{\Theta}_{c+}^{H}\boldsymbol{A}_{c1}^{H}\boldsymbol{A}_{c_1}\boldsymbol{\Theta}_{c-}\boldsymbol{\Upsilon}\end{bmatrix}\right)\end{aligned}\tag{A.4}$$

Referring to [22], (A.4) can be compactly expressed as

$$\boldsymbol{\Omega}=\boldsymbol{I}_2\otimes\left(\begin{bmatrix}j\boldsymbol{\Theta}_{u-}\boldsymbol{\Theta}_{u+}^{-1} & \boldsymbol{F}_1\\ \boldsymbol{0}_{L\times P} & \boldsymbol{F}_2\end{bmatrix}\right)\tag{A.5}$$

where

$$\begin{aligned}\begin{bmatrix}\boldsymbol{F}_1\\ \boldsymbol{F}_2\end{bmatrix} &= j\begin{bmatrix}\boldsymbol{\Theta}_{u+}^{H}\boldsymbol{A}_{u1}^{H}\boldsymbol{A}_{u1}\boldsymbol{\Theta}_{u+} & \boldsymbol{\Theta}_{u+}^{H}\boldsymbol{A}_{u1}^{H}\boldsymbol{A}_{c1}\boldsymbol{\Theta}_{c+}\boldsymbol{\Upsilon}\\ \boldsymbol{\Upsilon}^{H}\boldsymbol{\Theta}_{c+}^{H}\boldsymbol{A}_{c1}^{H}\boldsymbol{A}_{u1}\boldsymbol{\Theta}_{u+} & \boldsymbol{\Upsilon}^{H}\boldsymbol{\Theta}_{c+}^{H}\boldsymbol{A}_{c1}^{H}\boldsymbol{A}_{c1}\boldsymbol{\Theta}_{c+}\boldsymbol{\Upsilon}\end{bmatrix}^{-1}\\ &\quad\times\begin{bmatrix}\boldsymbol{\Theta}_{u+}^{H}\boldsymbol{A}_{u1}^{H}\boldsymbol{A}_{c1}\boldsymbol{\Theta}_{c-}\boldsymbol{\Upsilon}\\ \boldsymbol{\Upsilon}^{H}\boldsymbol{\Theta}_{c+}^{H}\boldsymbol{A}_{c1}^{H}\boldsymbol{A}_{c1}\boldsymbol{\Theta}_{c-}\boldsymbol{\Upsilon}\end{bmatrix}.\end{aligned}$$

Appendix B

In this appendix, we prove that the CA-matrix $\boldsymbol{B}$ defined in (26) is a centro-Hermitian matrix.

If $\boldsymbol{B}$ is a centro-Hermitian matrix, the equality $\boldsymbol{B}=\boldsymbol{J}_{M-G+1}\boldsymbol{B}^{*}\boldsymbol{J}_{4G}$ must hold.

$$\begin{aligned}\boldsymbol{J}_{M-G+1}\boldsymbol{B}^{*}\boldsymbol{J}_{4G} &= \boldsymbol{J}_{M-G+1}\left[\boldsymbol{Z}(\bar{m}),\boldsymbol{Z}(\bar{m})\boldsymbol{J}_G,\boldsymbol{J}_{M-G+1}\boldsymbol{Z}^{*}(\bar{m}),\right.\\ &\quad\left.\boldsymbol{J}_{M-G+1}\boldsymbol{Z}^{*}(\bar{m})\boldsymbol{J}_G\right]^{*}\boldsymbol{J}_{4G}\\ &= \left[\boldsymbol{J}_{M-G+1}\boldsymbol{Z}^{*}(\bar{m}),\boldsymbol{J}_{M-G+1}\boldsymbol{Z}^{*}(\bar{m})\boldsymbol{J}_G,\boldsymbol{Z}(\bar{m}),\right.\\ &\quad\left.\boldsymbol{Z}(\bar{m})\boldsymbol{J}_G\right]\boldsymbol{J}_{4G}\end{aligned}\tag{B.1}$$

Recalling that $[\boldsymbol{H}_1{:}\boldsymbol{H}_2{:}\boldsymbol{H}_3{:}\boldsymbol{H}_4]\boldsymbol{J}_{4G}=[\boldsymbol{H}_4\boldsymbol{J}_G{:}\boldsymbol{H}_2\boldsymbol{J}_G{:}\boldsymbol{H}_3\boldsymbol{J}_G{:}\boldsymbol{H}_4\boldsymbol{J}_G]$ and $\boldsymbol{J}_G\boldsymbol{J}_G=\boldsymbol{I}_G$, (B.1) can be rewritten as

$$\begin{aligned}\boldsymbol{J}_{M-G+1}\boldsymbol{B}^{*}\boldsymbol{J}_{4G} &= \left[\boldsymbol{Z}(\bar{m})\boldsymbol{J}_G\boldsymbol{J}_G,\boldsymbol{Z}(\bar{m})\boldsymbol{J}_G,\boldsymbol{J}_{M-G+1}\boldsymbol{Z}^{*}(\bar{m})\boldsymbol{J}_G\boldsymbol{J}_G,\right.\\ &\quad\left.\boldsymbol{J}_{M-G+1}\boldsymbol{Z}^{*}(\bar{m})\boldsymbol{J}_G\boldsymbol{J}_G\right]\\ &= \left[\boldsymbol{Z}(\bar{m}),\boldsymbol{Z}(\bar{m})\boldsymbol{J}_G,\boldsymbol{J}_{M-G+1}\boldsymbol{Z}^{*}(\bar{m}),\right.\\ &\quad\left.\boldsymbol{J}_{M-G+1}\boldsymbol{Z}^{*}(\bar{m})\right]=\boldsymbol{B}\end{aligned}\tag{B.2}$$

Appendix C

In this appendix, we derive the theoretical MSEs of DOA estimates for the uncorrelated and coherent sources given in (37) and (38).

For the kth uncorrelated source, the first-order derivative of (16) is taken as

$$\Delta\theta_{u_k}=\frac{\pi d}{\sqrt{\pi^2d^2-\lambda^2(\arctan\eta_k)^2}}\Delta\eta_k\tag{C.1}$$

Hence, the MSE of $\Delta\theta_{u_k}$ becomes

$$\begin{aligned}\mathrm{var}(\theta_{u_k}) &= E\left[(\hat{\theta}_{u_k}-\theta_{u_k})^2\right]=E\left[(\Delta\theta_{u_k})^2\right]\\ &= \frac{\pi^2d^2}{\pi^2d^2-\lambda^2(\arctan\eta_k)^2}E\left[(\Delta\eta_k)^2\right]\end{aligned}\tag{C.2}$$

To obtain the MSE of $\Delta\theta_{u_k}$, we should obtain the MSE of $\Delta\eta_k$ (i.e., $E[(\Delta\eta_k)^2]$) at first. Based on (14), we have

$$\begin{bmatrix}\boldsymbol{P}_1\boldsymbol{E}_s\\ \boldsymbol{P}_2\boldsymbol{E}_s\end{bmatrix}=\begin{bmatrix}\boldsymbol{P}_1\hat{\boldsymbol{A}}+\Delta\boldsymbol{A}_1\\ (\boldsymbol{P}_1\hat{\boldsymbol{A}}+\Delta\boldsymbol{A}_2)\boldsymbol{\Omega}\end{bmatrix}\boldsymbol{T}_s\tag{C.3}$$

As outlined in [32], by exploiting the first-order approximation for the Moore–Penrose inverse of $\boldsymbol{P}_1\hat{\boldsymbol{A}}+\Delta\boldsymbol{A}_1$, the least squares solution to $\tilde{\boldsymbol{\Omega}}$ is given by

$$\tilde{\boldsymbol{\Omega}} = \boldsymbol{T}_s^{-1}\big(\boldsymbol{I} + (\boldsymbol{P}_1\hat{\boldsymbol{A}})^{\dagger}(\Delta\boldsymbol{A}_2 - \Delta\boldsymbol{A}_1)\big)\boldsymbol{\Omega}\boldsymbol{T}_s \tag{C.4}$$

which implies that $\tilde{\boldsymbol{\Omega}}$ and $(\boldsymbol{I} + (\boldsymbol{P}_1\hat{\boldsymbol{A}})^{\dagger}(\Delta\boldsymbol{A}_2 - \Delta\boldsymbol{A}_1))\boldsymbol{\Omega}$ are similar matrices with respect to each other and share the same eigenvalues. With first-order perturbation approximation, the disturbance error of the kth eigenvalue $\Delta\eta_k$ is written as

$$\Delta\eta_k = \eta_k \boldsymbol{e}_k^T(\boldsymbol{P}_1\hat{\boldsymbol{A}})^{\dagger}(\Delta\boldsymbol{A}_2 - \Delta\boldsymbol{A}_1)\boldsymbol{e}_k \tag{C.5}$$

Then, the MSE of $\Delta\eta_k$ can be expressed as

$$E\big[(\Delta\eta_k)^2\big] = \eta_k^2\boldsymbol{e}_k^T(\boldsymbol{P}_1\hat{\boldsymbol{A}})^{\dagger}E\big[(\Delta\boldsymbol{A}_2 - \Delta\boldsymbol{A}_1)(\Delta\boldsymbol{A}_2 - \Delta\boldsymbol{A}_1)^T\big] \times \big(\boldsymbol{e}_k^T(\boldsymbol{P}_1\hat{\boldsymbol{A}})^{\dagger}\big)^T \tag{C.6}$$

By substituting (C.6) into (C.2), we have

$$\mathrm{var}(\theta_{u_k}) = \frac{\pi^2 d^2}{\pi^2 d^2 - \lambda^2(\arctan\eta_k)^2}\big(\eta_k^2\boldsymbol{e}_k^T(\boldsymbol{P}_1\hat{\boldsymbol{A}})^{\dagger} \times E\big[(\Delta\boldsymbol{A}_2 - \Delta\boldsymbol{A}_1)(\Delta\boldsymbol{A}_2 - \Delta\boldsymbol{A}_1)^T\big]\big(\boldsymbol{e}_k^T(\boldsymbol{P}_1\hat{\boldsymbol{A}})^{\dagger}\big)^T\big) \tag{C.7}$$

Here we choose $d = \lambda/2$ and (C.7) can be further simplified to

$$\mathrm{var}(\theta_{u_k}) = \frac{\pi^2}{-\frac{4}{9}\eta_k^4 + \frac{8}{3}\eta_k^2 - 4 + \pi^2\eta_k^{-2}}\big(\eta_k^2\boldsymbol{e}_k^T(\boldsymbol{P}_1\hat{\boldsymbol{A}})^{\dagger} \times E\big[(\Delta\boldsymbol{A}_2 - \Delta\boldsymbol{A}_1)(\Delta\boldsymbol{A}_2 - \Delta\boldsymbol{A}_1)^T\big]\big(\boldsymbol{e}_k^T(\boldsymbol{P}_1\hat{\boldsymbol{A}})^{\dagger}\big)^T\big) \tag{C.8}$$

where $E[(\Delta\boldsymbol{A}_2 - \Delta\boldsymbol{A}_1)(\Delta\boldsymbol{A}_2 - \Delta\boldsymbol{A}_1)^T] \approx \frac{1}{N}((\Delta\boldsymbol{A}_2 - \Delta\boldsymbol{A}_1)(\Delta\boldsymbol{A}_2 - \Delta\boldsymbol{A}_1)^T)$.

In a similar way as utilized in the derivation of $\mathrm{var}(\theta_{u_k})$, $\mathrm{var}(\theta_{c_k})$ can be expressed as

$$\mathrm{var}(\theta_{c_k}) = \frac{\pi^2}{-\frac{4}{9}\kappa_k^4 + \frac{8}{3}\kappa_k^2 - 4 + \pi^2\kappa_k^{-2}} \times \Big(\big(\boldsymbol{e}_k^T\big(\mathrm{Re}\big\{\boldsymbol{Q}_{M-G}^H\boldsymbol{K}_1^{M-G}\boldsymbol{Q}_{M-G+1}\big\}\big)^{\dagger} \times E\big[(\Delta\boldsymbol{K}_2 - \Delta\boldsymbol{K}_1)(\Delta\boldsymbol{K}_2 - \Delta\boldsymbol{K}_1)^T\big] \times \big(\boldsymbol{e}_k^T\big(\mathrm{Re}\big\{\boldsymbol{Q}_{M-G}^H\boldsymbol{K}_1^{M-G}\boldsymbol{Q}_{M-G+1}\big\}\big)^{\dagger}\big)^T\Big)\Big) \tag{C.9}$$

with $E[(\Delta\boldsymbol{K}_2 - \Delta\boldsymbol{K}_1)(\Delta\boldsymbol{K}_2 - \Delta\boldsymbol{K}_1)^T] \approx \frac{1}{N}((\Delta\boldsymbol{K}_2 - \Delta\boldsymbol{K}_1)(\Delta\boldsymbol{K}_2 - \Delta\boldsymbol{K}_1)^T)$.

Appendix D. Supplementary material

Supplementary material related to this article can be found online at http://dx.doi.org/10.1016/j.dsp.2016.07.024.

References

[1] H. Krim, M. Viberg, Two decades of array signal processing research: the parametric approach, IEEE Signal Process. Mag. 13 (4) (1996) 67–94.
[2] Z. Weng, P.M. Djurić, A search-free DOA estimation algorithm for coprime arrays, Digit. Signal Process. 24 (2014) 27–33.
[3] B. Ottersten, M. Viberg, P. Stoica, A. Nehorai, Exact and large sample maximum likelihood techniques for parameter estimation and detection in array processing, Springer, Berlin, Heidelberg, 1993, pp. 99–151.
[4] R.O. Schmidt, Multiple emitter location and signal parameter estimation, IEEE Trans. Antennas Propag. 34 (3) (1986) 276–280.
[5] R.H. Roy, T. Kailath, ESPRIT-estimation of signal parameters via rotational invariance techniques, IEEE Trans. Acoust. Speech Signal Process. 37 (7) (1989) 984–995.
[6] L. Wan, G. Han, J.J.P.C. Rodrigues, W. Si, An energy efficient DOA estimation algorithm for uncorrelated and coherent signals in virtual MIMO systems, Telecommun. Syst. 59 (1) (2015) 93–110.
[7] J.E. Evans, J.R. Johnson, D.F. Sun, High resolution angular spectrum estimation techniques for terrain scattering analysis and angle of arrival estimation, in: Proceedings of 1st ASSP Workshop Spectral Estimation, 1981, pp. 134–139.
[8] T.J. Shan, M. Wax, T. Kailath, On spatial smoothing for direction-of-arrival estimation of coherent signals, IEEE Trans. Acoust. Speech Signal Process. 33 (4) (1985) 806–811.
[9] S.U. Pillai, B.H. Kwon, Forward/backward spatial smoothing techniques for coherent signal identification, IEEE Trans. Acoust. Speech Signal Process. 37 (1) (1989) 8–15.
[10] R. Rajagopal, P.R. Rao, Generalised algorithm for DOA estimation in a passive sonar, IEE Proc., F, Radar Signal Process. 140 (1) (1993) 12–20.
[11] C. Qi, Y. Wang, Y. Zhang, Y. Han, Spatial difference smoothing for DOA estimation of coherent signals, IEEE Signal Process. Lett. 12 (11) (2005) 800–802.
[12] F. Liu, J. Wang, C. Sun, R. Du, Spatial differencing method for DOA estimation under the coexistence of both uncorrelated and coherent signals, IEEE Trans. Antennas Propag. 60 (4) (2012) 2052–2062.
[13] Z. Ye, X. Xu, DOA estimation by exploiting the symmetric configuration of uniform linear array, IEEE Trans. Antennas Propag. 55 (12) (2007) 3716–3720.
[14] X. Xu, Z. Ye, Y. Zhang, C. Chang, A deflation approach to direction of arrival estimation for symmetric uniform linear array, IEEE Antennas Wirel. Propag. Lett. 5 (1) (2006) 486–489.
[15] X. Xu, Z. Ye, J. Peng, Method of direction-of-arrival estimation for uncorrelated, partially correlated and coherent sources, IET Microw. Antennas Propag. 1 (4) (2007) 949–954.
[16] X. Xu, Z. Ye, Y. Zhang, DOA estimation for mixed signals in the presence of mutual coupling, IEEE Trans. Signal Process. 57 (9) (2009) 3523–3532.
[17] H. Tao, J. Xin, J. Wang, N. Zheng, Two-dimensional direction estimation for a mixture of noncoherent and coherent signals, IEEE Trans. Signal Process. 63 (2) (2015) 318–333.
[18] Z. Ye, Y. Zhang, C. Liu, Direction-of-arrival estimation for uncorrelated and coherent signals with fewer sensors, IET Microw. Antennas Propag. 3 (3) (2009) 473–482.
[19] L. Gan, X. Luo, Direction-of-arrival estimation for uncorrelated and coherent signals in the presence of multipath propagation, IET Microw. Antennas Propag. 7 (9) (2013) 746–753.
[20] H. Shi, W. Leng, A. Wang, T. Guo, DOA estimation for mixed uncorrelated and coherent sources in multipath environment, Int. J. Antennas Propag. (2015) 1–8.
[21] E. BouDaher, F. Ahmad, M.G. Amin, Sparsity-based DOA estimation of coherent and uncorrelated targets using transmit/receive co-prime arrays, in: SPIE Sensing Technology + Applications, International Society for Optics and Photonics, 2015, 94840E, 6 pp.
[22] Y. Zhang, Z. Ye, C. Liu, An efficient DOA estimation method in multipath environment, Signal Process. 90 (2) (2010) 707–713.
[23] K.C. Huarng, C.C. Yeh, A unitary transformation method for angle-of-arrival estimation, IEEE Trans. Signal Process. 39 (4) (1991) 975–977.
[24] G. Zheng, B. Chen, M. Yang, Unitary ESPRIT algorithm for bistatic MIMO radar, Electron. Lett. 48 (3) (2012) 179–181.
[25] Q. Huang, R. Hu, Y. Fang, Real-valued MVDR beamforming using spherical arrays with frequency invariant characteristic, Digit. Signal Process. 48 (2016) 239–245.
[26] C. Qian, L. Huang, H.C. So, N.D. Sidiropoulos, J. Xie, Unitary PUMA algorithm for estimating the frequency of a complex sinusoid, IEEE Trans. Signal Process. 63 (20) (2015) 5358–5368.
[27] C. Qian, L. Huang, Y. Xiao, H.C. So, Two-step reliability test based unitary root-MUSIC for direction-of-arrival estimation, Digit. Signal Process. 44 (2015) 68–75.
[28] N. Yilmazer, J. Koh, T.K. Sarkar, Utilization of a unitary transform for efficient computation in the matrix pencil method to find the direction of arrival, IEEE Trans. Antennas Propag. 54 (1) (2006) 175–181.
[29] F.G. Yan, M. Jin, S. Liu, X.L. Qiao, Real-valued MUSIC for efficient direction estimation with arbitrary array geometries, IEEE Trans. Signal Process. 62 (6) (2014) 1548–1560.
[30] T.J. Shan, A. Paulraj, T. Kailath, On smoothed rank profile tests in eigenstructure methods for directions-of-arrival estimation, IEEE Trans. Acoust. Speech Signal Process. 35 (10) (1987) 1377–1385.
[31] Y. Zhang, Z. Ye, C. Liu, Estimation of fading coefficients in the presence of multipath propagation, IEEE Trans. Antennas Propag. 57 (7) (2009) 2220–2224.
[32] V.C. Soon, Y.F. Huang, An analysis of ESPRIT under random sensor uncertainties, IEEE Trans. Signal Process. 40 (9) (1992) 2353–2358.
[33] G. Golub, C. van Loan, Matrix Computations, vol. 3, Johns Hopkins University Press, Baltimore, ML, USA, 1996.

Wei-Jian Si was born in Beijing. He received the B.E. degree from Beihang University and the Ph.D. degree from Harbin Engineering University in 1994 and 2004. From 1995 to 1999, he joined the 35th institute of China Aerospace Science and Industry Corporation and was engaged in scientific research on radar signal processing. He is currently a professor and Ph.D. supervisor at College of Information and Communication Engineering, Harbin Engineering University, Heilongjiang, China. His main research interests include radar signal detection, processing and identification, high precision passive direction finding and spatial spectrum estimation.

Pin-Jiao Zhao was born in Heilongjiang on June 25, 1990. She received the B.E. degree from Harbin Engineering University, Heilongjiang, China, in 2013. She is currently pursuing the Ph.D. degree in the field of Information and Communication Engineering at Harbin Engineering University. Her research interests include array signal processing and its applications.

Zhi-Yu Qu was born in Jilin. She received the Ph.D. degree in Communication and Information System from Harbin Engineering University, Heilongjiang, China, in 2008. From 2009 to 2013, she joined Nanjing Research Institute of Electronic Technology and was engaged in scientific research on radar signal processing and its applications. She is currently an associate professor at Harbin Engineering University. Her current research interests are radar signal processing, high precision passive direction finding and multiple target tracking.

Yan Wang was born in Henan on April 29, 1992. He received the B.E. degree in Electronic Information Engineering from Harbin Engineering University, Heilongjiang, China, in 2013. He is currently pursuing the Ph.D. degree in the field of Information and Communication Engineering at Harbin Engineering University. His research interests include high precision passive direction finding and its applications.